May 2022

SARS-CoV-2 RNA Persistence in Municipal Wastewater Treatment Systems Proves Wastewater Surveillance Is an Effective Tool for Monitoring COVID-19 Community Health Burdens

Melissa K. Schussman
University of Wisconsin-Milwaukee

SARS-CoV-2 RNA PERSISTENCE IN MUNICIPAL WASTEWATER TREATMENT SYSTEMS PROVES WASTEWATER SURVEILLANCE IS AN EFFECTIVE TOOL FOR MONITORING COVID-19 COMMUNITY HEALTH BURDENS

by

Melissa Schussman

A Thesis Submitted in

Partial Fulfillment of the

Requirements for the Degree of

Master of Science

in Engineering

at

The University of Wisconsin-Milwaukee

May 2022

ABSTRACT

SARS-CoV-2 RNA PERSISTENCE IN MUNICIPAL WASTEWATER TREATMENT SYSTEMS PROVES WASTEWATER SURVEILLANCE IS AN EFFECTIVE TOOL FOR MONITORING COVID-19 COMMUNITY HEALTH BURDENS

by

Melissa Schussman

The University of Wisconsin Milwaukee, 2022
Under the Supervision of Professor Sandra McLellan

Wastewater surveillance of SARS-CoV-2 is used worldwide to track COVID-19 infection trends. However, there is no standard method for SARS-CoV-2 measurement from wastewater, and uncertainties of pre-analytical influences from the wastewater collection system persist. This study builds upon the growing body of knowledge surrounding wastewater surveillance and aims to understand how wastewater measurements relate to other public health metrics, explain the influence of wastewater conveyance systems, and improve SARS-CoV-2 detection and quantification from wastewater.

Our laboratory has been part of the ongoing Wisconsin SARS-CoV-2 wastewater surveillance program since August 2020, analyzing almost 4,000 samples to date. Through various experiments, our findings demonstrated that monitoring variants in wastewater using RT-ddPCR can outperform clinical sequencing. Temperature was the only parameter that significantly influenced SARS-CoV-2 decay in the wastewater matrix. Travel time, flow rate, BOD, and TSS, did not significantly influence SARS-CoV-2 decay or detection. Additionally, extracting RNA from primary settled solids improved detection sensitivity.

TABLE OF CONTENTS

LIST OF FIGURES

LIST OF TABLES

LIST OF ABBREVIATIONS

COVID-19	coronavirus disease 2019
SARS-CoV-2	severe acute respiratory syndrome coronavirus 2
MMSD	Milwaukee Metropolitan Sewage District
PCR	polymerase chain reaction
PMMoV	Pepper Mild Mottle Virus
BCoV	Bovine Coronavirus
BRSV	Bovine Respiratory Syncytial Virus
RT-ddPCR	reverse transcription droplet digital PCR
WWTP	wastewater treatment plant
MG	million gallons
MGD	million gallons per day
BRK	Brookfield wastewater treatment plant
CED	Cedarburg wastewater treatment plant
PLT	Green Bay wastewater treatment plant
DP	De Pere wastewater treatment plant
JI	Jones Island Water Reclamation Facility
SS	South Shore Water Reclamation Facility
ORE	Oregon wastewater treatment plant
RAC	Racine wastewater treatment plant
WAU	Waukesha wastewater treatment plant
rpm	revolutions per minute
NTC	no template control
LOD	limit of detection
LOQ	limit of quantification
DHS	Department of Health Services
BOD	Biological Oxygen Demand
TSS	Total suspended solids

ACKNOWLEDGEMENTS

This research would have been possible without the cooperation and assistance of numerous people. I would first like to express my sincere gratitude to my advisor, Professor Sandra McLellan for her continuous support of my academic journey, immense knowledge, and dedicated involvement in my research. It is rare to find a mentor like you, who has the ability to compel constant improvement, while simultaneously allowing me to feel genuinely appreciated for my efforts. I am extremely appreciative of my committee members expertise, and assistance with this project. Professor Hector Bravo, you were unquestionably instrumental to my travel time analysis, your meticulous review of my manuscript provided an impact that is obvious throughout this paper. Professor Yin Wang, your assistance goes beyond my thesis, I gratefully acknowledge your support throughout my transition into graduate school.

I am deeply indebted to Adelaide Roguet, who provided endless technical support, vast knowledge, and unwavering encouragement in not only this project, but in various aspects of my life. I would like to thank Shuchen Feng for teaching me the art of the RT-ddPCR and being patient with me as I was learning such an articulate instrument. I also thank Brooke Dinan and Angie Schmoldt for offering me endless assistance with the COVID-19 project, even during odd hours, holiday weekends, or truly whenever their expertise was needed. I would like to acknowledge my lab mates Brigid Meyers, Lexi Passante, Deb Dila, Brenden Nihart, and Melinda Bootsma, who were always quick to offer support in the laboratory, advice on presentations, and an editorial eye on papers.

I would also like to acknowledge Jonathan Meiman, Nathan Kloczko, and Mathew Schinwald from Wisconsin DHS, and the COVID-19 wastewater surveillance team Kayley Janssen, Dagmara Antkiewicz, Martin Shafer, and Jocelyn Hemming at the Wisconsin State

Laboratory of Hygiene for insightful discussion and sharing of knowledge. I would like to thank all the wastewater treatment plants that provided samples and timely data to our laboratory each week. I would like to acknowledge MMSD for not only providing samples and sharing expertise about individual systems, but specifically Tom Simmons, Joe Lesczynski, Emily Herda, and Matt Magruder for compiling, providing, and helping to interpret data used in my travel-time analysis.

Lastly, I would like to thank my family and friends for their constant patience and support with my ever-evolving career goals. Specifically, my parents who instilled in me the belief I am capable of anything I put my mind to. My partner, who bore the weight of always being the first person to whom I unburdened my academic woes. And my closest friends, who have always been there to provide inspiring discussions and refreshing distractions to rest my mind outside of my academic life. This research would not have been possible without their encouragement to both begin and complete this journey.

Chapter 1: Literature Review and Background

1.1 Protection of human health

Looking at a broad evaluation of human health, The World Health Organization (WHO), an agency of the United Nations, attests the human right to the highest attainable standard of health [1]. The core elements to this right are requiring governments to take immediate steps towards fulfilling the highest attainable standard of health when necessary and to not reduce already-in-place protection of economic, social, and cultural rights. The core components of the right to health are sufficiently available, accessible, and quality health care, goods, services, and programs that are acceptable for all people requiring such resources [2]. WHO also helps enforce the right to human health by developing global strategies against preventing and controlling certain diseases of concern [3].

Focusing on human health in the United States (US), the US Department of Health and Human Services (HHS) is a federal agency that was created to enhance the health and well-being of all Americans by providing services and advances in medicine, public health, and social science [4]. HHS has 11 operating divisions, one of which is the US Centers for Disease Control and Prevention (CDC) to protect our country's citizens from health and safety threats by conducting experimentation, providing health information, and responding accordingly to health threats [5].

1.2 COVID-19

The newly discovered coronavirus disease 2019 (COVID-19) disease is a highly contagious disease that was submerged originally from a bat coronavirus. Coronaviruses are a

family of large enveloped positive-strand RNA viruses that infect vertebrates [6]. COVID-19 was first identified in Wuhan, China in December 2019, and has since spread worldwide, leading to WHO declaring the COVID-19 outbreak as a pandemic on March 11, 2020 [7]. As of March 24, 2022, in the United States alone, over 81 million cases have been confirmed, with more than 1 million deaths resulting from COVID-19 [8]. This disease is spread through droplets or direct contact with an infected individual [9]. Clinical presentations of COVID-19 range from asymptomatic or mild symptoms to severe illness and mortality [10]. The incubation period of COVID-19 ranges from 2 to 14 days, with an average of 5, after which, symptoms begin [11]. Characteristic symptoms of COVID-19 are similar to a common cold, or flu; including fever, headache, and respiratory symptoms such as cough, difficulty breathing, sore throat, and congestion [12]. But while infected patients typically present respiratory symptoms, studies have shown that up to 35% of confirmed cases display gastrointestinal symptoms, such as diarrhea, vomiting, and abdominal pain [5], [26], [28]. Due to asymptomatic and oligosymptomatic cases in addition to limited testing availability, there is uncertainty surrounding the number of diagnosed cases [13]. While current testing is being performed using nasopharyngeal and oropharyngeal swabs, recent studies have also shown that stool samples can result in more accurate detection of COVID-19 as it is shed in feces in concentrations up to 10^7 copies per gram [23]. Positive fecal samples remained positive for an average of 12.5 days after respiratory samples became negative, and in 1% of cases, infection would not have been diagnosed with respiratory testing alone [25], [26].

1.2.1 SARS-CoV-2 RNA

The severe acute respiratory syndrome coronavirus 2 (SARS-CoV-2) is the causative agent of COVID-19. It is an enveloped non-segmented positive-sense ribonucleic acid (RNA) that belongs to the species *Severe acute respiratory syndrome-related coronavirus* and the genus *Betacoronavirus* (Figure 1) [6]. Key distinguishing features of the SARS-CoV-2 genome that make it so threatening to human health are a polybasic furin cleavage site that may increase infectivity by enhancing cell to cell fusion without affecting viral entry, and O-linked glycans that can cover epitopes, making it harder for the immune system to attack this foreign substance [14].

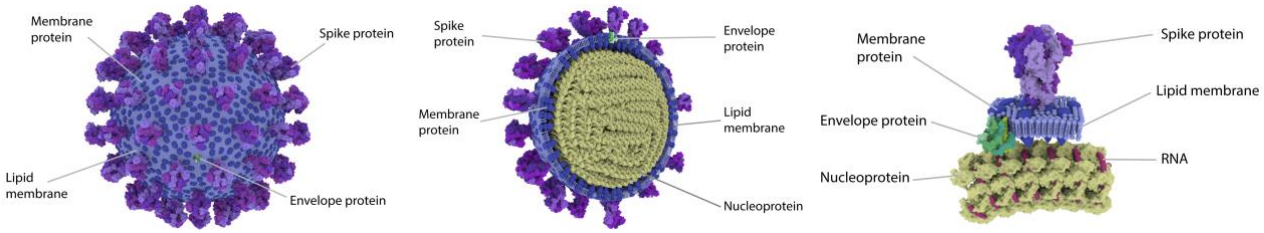

Figure 1. 3-D model of the morphology of SARS-CoV-2 created by Gaslow Life Sciences [15].

1.3 Wastewater Surveillance

Wastewater surveillance is a public health tool involving extracting endogenous and exogenous human biomarkers from a wastewater sample, then detecting, analyzing, and interpreting specific compounds or molecules [15]. This method has been researched and applied as a large population surveillance method for detecting and monitoring viral pathogens and viruses [16], that can provide comprehensive health information on communities in real-time [15], and unlike traditional clinical testing, one sample can be used to target numerous viruses or pathogens. Wastewater surveillance provides an unbiased reflection of community health accounting for a wide range of people who may often be missed or misrepresented by medical

testing alone and can be used by health officials to rapidly assess emerging threats, and prepare for pandemics [17].

1.3.1 Wastewater

Approximately 80% of US households are served by municipal wastewater collection systems, permitting fecal waste to arrive at a wastewater treatment plant within just a few hours [17]. This wastewater influent reflects an integrated profile of the human population microbiome within the community contributing waste into the treatment system [18]. Wastewater has an extremely multifaceted and dynamic composition, that varies depending on location, time of the year, weather, and individual pollutants from industrial, urban, environmental, and residential sources [19]. Sixty-five toxic and priority pollutants, among various others, are monitored in wastewater effluent under the Code of Federal Regulations (CFR), but the true composition of wastewater at any given time is unknown [19].

1.3.2 Methodological Considerations

Because wastewater is such a complex matrix, it can be challenging to get a sample that contains enough concentration for target detection. There are peak times associated with higher residential water usage such as mornings due to showers, and evenings due to washing machine, or dishwasher use [20], [21]. In addition, environmental factors, such as a severe rain event, or snowmelt can lead to an overdiluted sample. It is important to take these such events into account when collecting samples. A measure used to assess possible dilution of a sample is to test each sample for human fecal indicators, such as Pepper Mild Mottle Virus (PMMoV) which is an extremely common RNA virus found in human fecal waste as a result of eating peppers

[22]. Using a human-specific fecal marker in the sample processing can better quantify the number of people contributing to a sewershed, can be used as a comparative measure between samples over time, and can help account for viral losses throughout the wastewater conveyance or laboratory processes [23].

In addition to sample dilution, there are many contaminants that can interfere with the target compound in wastewater analysis. The abundance of biological and chemical substances in wastewater makes it harder to successfully extract the target biomarker and may cause inhibition of detection even when successfully extracting a specific biomarker [15]. To avoid undetected inhibition, an inhibition control may be necessary. This involves spiking polymerase chain reaction (PCR) aliquots with a non-native molecular target, and confirming this target can be detected when the plate is read [24]. It may also be necessary to use blind matrix spikes, which involve spiking wastewater samples with a surrogate virus to measure viral RNA recovery during the extraction process [24], [25].

1.3.3 SARS-CoV-2 Analysis

The discovery of fecal shedding of SARS-CoV-2 prompted worldwide experimentation of quantifying SARS-CoV-2 through wastewater surveillance [26]. While there is currently no single standard method for analyzing SARS-CoV-2 in wastewater, studies have been conducted by multiple laboratories underneath the Water Research Foundation (WRF) and National Wastewater Surveillance System (NWSS) to identify reliable, reproducible, and sensitive methods [24][17]. This work has so far concluded that while various methods of RNA extraction can be used, all laboratories will analyze the SARS-CoV-2 molecular signal via PCR using the N1 and N2 gene target primer and probe sets designed by the CDC (Table 1)[24]. NWSS has

also concluded that the limit of detection for SARS-CoV-2 is yet to be properly established, and therefore, wastewater surveillance cannot be used to determine if a community if free from SARS-CoV-2 infection [17]. Wastewater surveillance is still considered a valuable resource, as per capita incidence of COVID-19 can be estimated within a community through surveillance data, daily wastewater flow rates, and population number [27].

Table 1. Primers and Probes used for RT-ddPCR reactions. *

Target	Primer/Probe Sequence (5'-3')	Supplier	Ref
SARS-CoV-2 N1	F: GACCCCAAAATCAGCGAAAT	Eurofins	[28]
	R: TCTGGTTACTGCCAGTTGAATCTG	Eurofins	
	P: FAM/ACCCCGCAT/ZEN/TACGTTTGGTGGACC/lABkFQ	IDT	
SARS-CoV-2 N2	F: TTACAAACATTGGCCGCAAA	Eurofins	[28]
	R: GCGCGACATTCCGAAGAA	Eurofins	
	P: HEX/ACAATTTGCCCCCAGCGCTTCAG/BHQI and HEX/ACAATTTGC/ZEN/CCCCAGCGCTTCAG/lABkFQ	IDT	
BCoV	F: CTGGAAGTTGGTGGAGTT	IDT	[29]
	R: ATTATCGGCCTAACATACATC	IDT	
	P: /FAM/CCTTCATAT/ZEN/CTATACACATCAAGTTGTT/IA BkFQ/	IDT	
BRSV	F: GCAATGCTGCAGGACTAGGTATAAT	IDT	[30]
	R: ACACTGTAATTGATGACCCCATTCT	IDT	
	P: /HEX/ACCAAGACT/ZEN/AGTATGATGCTGCCAAAGCA/I ABkFQ/	IDT	
PMMoV	F: GAGTGGTTTGACCTTAACGTTGA	IDT	[31]
	R: TTGTCGGTTGCAATGCAAGT	IDT	
	P: FAM/CCTACCGAAGCAAATG/MGBNFQ/	Applied Biosystems	

* Bovine Coronavirus indicated as BCoV, Bovine Coronavirus indicated as BRSV

1.4 Literature Gap and Research Contributions

In addition to wastewater variables, there are still uncertainties around SARS-CoV-2 RNA. The most pertinent uncertainties include: the rate and mass of virus RNA shedding in feces during all phases of symptomatic and asymptomatic COVID-19 phases; the influence of facility and sewershed-specific factors contributing to the wastewater matrix; and the virus survival and persistence in the sewer and laboratory [32]. Fecal virus shedding has been the

center of frequent debate since SARS-CoV-2 wastewater surveillance began. There are various studies attempting to solve this question, however the most promising conclusion is that the shedding of SARS-CoV-2 can vary greatly between positive COVID-19 patients. While one study has proven 100% of COVID-19 positive patients shed fecal SARS-CoV-2 [33], the average prevalence of COVID-19 positive patients that shed fecal SARS-CoV-2 RNA is closer to 50% [34]. Of the patients that did shed SARS-CoV-2 in fecal matter, there was no significant difference in shedding when comparing severity of the disease, or age of the patient [35]. However, patients with GI symptoms were almost twice as likely to exhibit fecal shedding than patients who did not experience any GI related symptoms [36].

There is also uncertainty on how long of a period does SARS-CoV-2 RNA sheds. Many studies have illustrated that SARS-CoV-2 RNA in feces can be detected for a longer duration than respiratory and serum samples [26], [37]–[41] averaging around 22 days from the onset of symptoms [34], [38]. This may result is a slight offset of the relationship of SARS-CoV-2 detected in wastewater, and clinical case rate. Assessments on SARS-CoV-2 fecal shedding are oh high-priority, and are currently being performed by the clinical sector [42].

Other high-priority research opportunities declared by the WRF are effect of wastewater pretreatment on genetic signal, and dilution or persistence of the genetic signal in the sewer collection system [42]. Specific parameters in the sewer collection system that have a known influence on viral RNA, and are assumed to have an impact on SARS-CoV-2 detection in wastewater include pH, temperature, organic matter, solids content, residence time in the sewer, sampling, and microbial antagonism [43]–[45].

1.5 Goals and Objectives

This research seeks to provide information that can help fill gaps in current literature and process's encompassing wastewater surveillance of COVID-19. The main goal of this work is to determine the impacts wastewater has on viral RNA to see how wastewater surveillance can be more efficiently used for public health, and to confirm that it is a reliable metric. In doing this, my research will cover three specific aims:

Specific aim 1: Analyze how wastewater data used for wastewater surveillance relate to other public health metrics.

Specific aim 2: Explain the influence of wastewater conveyance systems on SARS-CoV-2 virus survival and detectability by examining the relationships SARS-CoV-2 RNA concentration has with wastewater parameters such as travel time, temperature, BOD, TSS, and average daily flow rate.

Specific aim 3: Improve detection and quantification of SARS-CoV-2 for wastewater surveillance using knowledge on the effects of parameters explored in previous chapters.

To answer these questions data analysis and experimentation will be performed in addition to UW- Milwaukee's weekly COVID-19 surveillance program that had been ongoing since August 2020. Prior to any analysis performed for this thesis, we were already aware that the COVID-19 trends detected from our wastewater surveillance data is significantly correlated to the clinical COVID-19 case rate within that community [46] (Figure 2). The objective of Chapter 3 is to assess how wastewater surveillance compares to other public health tools that are being used for COVID-19. This was done by comparing data obtained from seven WWTP's

using reverse transcription droplet digital PCR (RT-ddPCR) on the Omicron variant to clinical sequenced data. The objective of Chapter 4 is to determine if there is a measurable impact of SARS-CoV-2 decay in wastewater throughout the residence time of an average sewer network. To do this, SARS-CoV-2 loads from two interconnected sewer service areas with different travel times were compared. Travel time was determined based off of metered velocity values, and various parameters were analyzed for a correlation to SARS-CoV-2 load. The objective of Chapter 5 is to determine possible improvements to COVID-19 wastewater surveillance based off of results from SARS-CoV-2 persistence and decay analyses. To do this, SARS-CoV-2 concentrations from Jones Island Water Reclamation Facility (JI) sludge samples were directly compared to wastewater influent from the same collection date to determine if signal of detection could be increased or improved to better benefit public health.

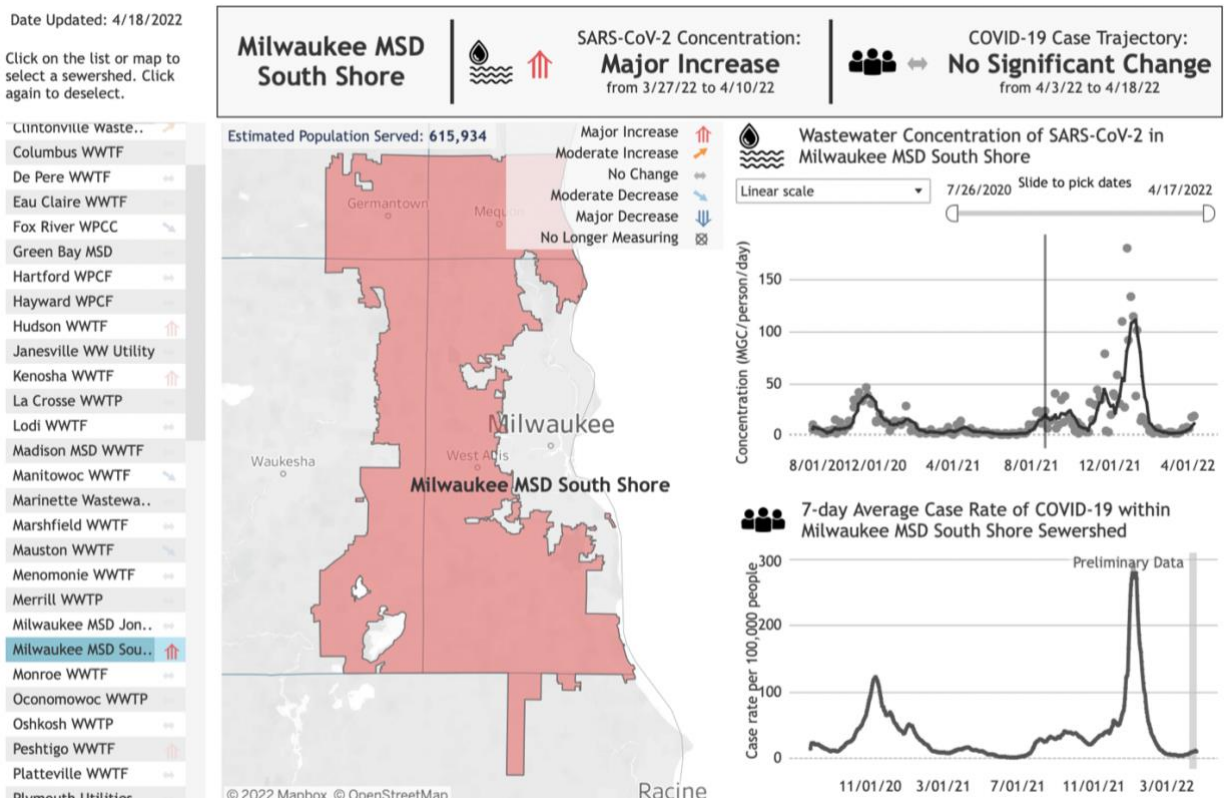

Figure 2. Screenshot of the Wisconsin Department of Health Services (DHS) dashboard to illustrating correlating data of COVID-19 infection trends in wastewater surveillance (top graph), and clinical case data (bottom graph) in the SS WWTP service area.

Collectively, these results add knowledge and understanding to wastewater surveillance, and can aid researchers when determining the best way to analyze and report data obtained from wastewater surveillance programs. The overarching goal of this study is to reduce uncertainty within this public health tool, and to contribute evidence that wastewater surveillance is an effective method in tracking new and spreading diseases that can offer a wide spectrum of applications for public health.

Chapter 2: General Materials and Methodology

2.1 Collection of Influent Samples

Sewage influent samples were collected between August 30, 2020, and February 28, 2022, from nine wastewater treatment plants (WWTP) across Wisconsin, United States (Table 2). Flow-weighted 24-hour composite samples were collected twice per week, unless specified in Table 2, by each WWTP according to the plant standard collection procedures and then transferred to 500 mL bottles. Samples were stored at 4°C until shipped overnight on ice. Upon arrival at the laboratory, samples were immediately stored at 4°C before processing within 24 hours. Influent chemical and physical measurements were provided by WWTP operators employing their routine procedures for each sample.

Table 2. Operating Conditions of all WWTP's used throughout this paper.[a]

WWTP	County	Sample Frequency*	Population Served	Capacity (MGD)	Average Flow (MGD)	Composite Frequency (MG)
Brookfield (BRK)	Waukesha	2 x per week	51000	13	8 ± 1	0.35
Cedarburg (CED)	Ozaukee	1x per week	12000	3	2 ± 0	0.02
Green Bay (PLT)	Brown	2 x per week	189000	49	24 ± 4	0.09
De Pere (DP)	Brown	2 x per week	43000	14	7 ± 1	0.02
Jones Island (JI)	Milwaukee	2 x per week	470000	330	75 ± 23	0.56 - 0.65
South Shore (SS)	Milwaukee	2 x per week	616000	300	74 ± 17	1.7
Oregon (ORE)	Dane	1x per week	10000	2	1 ± 0	0.05
Racine (RAC)	Racine	2 x per week	139000	36	15 ± 4	0.08
Waukesha (WAU)	Waukesha	2 x per week	73000	39	7 ± 1	0.1

*CED and ORE only collected once per week

[a]MGD is million gallons per day, MG is million gallons

2.2 Processing Influent Samples

2.2.1 Pre-analytical processing

Wastewater samples were shaken vigorously until visually well-mixed, then 25 mL of each sample were pipetted into 50 mL conical tubes containing 250 µL magnesium chloride solution ($MgCl_2$) to reach a final concentration of 25 mM. The presence of salts such as $MgCl_2$ can enhance virus adsorption to cellulose ester membranes [47]. Approximately 100,000 copies (5 µL) of BCoV were spiked into the solution to act as a recovery control, then the mixture is poured into a magnetic filter funnel containing a 0.8 µm 47 mm diameter esters HA filter (MF-Millipore, Carrigtwohill, Ireland). Samples were filtered at a low vacuum (~50 mmHg VAC) until no pooled liquid is visible on the filter. Once the filtering was complete, the filter was folded, and put into a 2 mL ZR BashingBead Lysis Tube (Zymo, Irvine, CA, USA) containing buffer solution relevant to nucleic extraction protocol (Chapters 2.2.2-2.2.4).

2.2.2 Qiagen RNA Extraction Preparation

All samples prior to August 25, 2021, were extracted according to the RNeasy PowerMicrobiome Kit (Qiagen, Hilden, Germany). The tube containing the filter and 650 µL of PM1(PowerMicrobiome Kit by Qiagen) buffer solution are stored at -80°C for minimum of two hours to improve RNA extraction yield. Once removed from the -80°C freezer, while still frozen, the samples are spiked with 6.5 µL β-mercaptoethanol and allowed to completely thaw before bead-beating for 2.5 minutes, resting on ice for 5 minutes, then repeating to properly break-up the filter. The samples are extracted following the RNeasy PowerMicrobiome Kit (Table 3) Handbook with minor alternations, as explained in section 2.2.3.

2.2.3 Qiagen RNA Extraction

All centrifugation for extraction is performed at room temperature at 150,000 revolutions per minute (rpm) for one minute unless specified otherwise. After bead-beating, the samples were centrifuged, and 450 µL of the supernatant was transferred to a Collection Tube.150 µL of Solution IRS was spiked into the tube, vortexed briefly to mix, and incubated at 2–8°C for 5 minutes. After incubation, the samples were centrifuged, and avoiding the pellet, 650 µL of the supernatant was transferred to a new Collection Tube. 650 µL of both Solution PM3 and Solution PM4 were spiked and inverted until visually clear. 650 µL of the mixture was transferred into an MB Spin Column and centrifuged, discarding flow-through and repeating until all of the mixture passed through the MB Spin Column. 650 µL of Solution PM5 was loaded into the MB Spin Column and centrifuged. The flow-through was discarded, and 600 µL of Solution PM4 was transferred into the spin column. The samples were centrifuged, the flow-through is discarded, then samples are centrifuged for an additional 2 minutes at room temperature. The MB Spin Column was transferred to a clean 2 mL Collection Tube, and 60 µL of warm RNase-Free Water was added to the center of the MB Spin Column membrane. The samples were incubated at room temperature for 5 minutes and centrifuged. The 60mL flow-through elution was transferred into a 0.5 mL Low Adhesion Surface Micrew Tube (Simport Scientific, Bernard-Pilon Beloeil, QC Canada), and was frozen immediately at -80°C to preserve RNA, until analyzed on RT-ddPCR.

Table 3. components of RNeasy PowerMicrobiome Kit (Qiagen, Catalog number 26000-50)

Component	Amount per Kit
PowerBead Tube, Gloss O. 1 mm	50
Solution PM1	55 mL
Solution IRS	15 mL
Solution PM3	36 mL
Solution PM4	3 x 24 mL
Solution PM5	3 x 30 mL
DNase Digestion Solution	2 x 1.5 ml
Solution PM7	23 ml
RNase-Free Water	10 ml
DNase I (RNase-free)	1 vial (1500 units)
MB RNA Spin Columns	50
Collection Tubes (2 ml)	4 x 50

2.2.4 KingFisher RNA extraction

All samples after August 25, 2021, were extracted using a custom Maxwell® HT Environmental TNA Kit (Promega, Madison, WI, USA) (Table 4) on an automated KingFisher Flex instrument (ThermoFisher Scientific, Waltham, MA). Samples were thawed completely on ice before bead bead-beating for 2.5 minutes, resting on ice for 5 minutes, then repeating to properly break up the filter. Six purification plates were made prior to running the instrument: two wash plates containing 100 µL of 50% ethanol and 900 µL of wash buffer (WBA) required for purification, an Ethanol Wash plate with 450µl of 50% ethanol required for purification, an elution plate with 100 µL of 25 mM Tris-HCl (pH 8.0), a plate containing KingFisher 96-tip comb for reagent and sample transfer, and a Lysis and Bind plate containing 35 µL of Resin, 50 µL of Alkaline Protease solution (APA), 250 µL of cell lysis solution (CLD), 400 µL of Isopropanol (100%) to each well required for purification. 250 µL of all sample supernatant except SS (125 µL) was added to the lysis and bind plate. This instrument mixes the samples while heating to complete lysis, then binds nucleic acid to the resin, washes the resin, dries the

resin, and completes elution of the sample. The 100 µL elution was transferred into a 0.5 mL Low Adhesion Surface Micrew Tube (Simport Scientific, Bernard-Pilon Beloeil, QC Canada), and was frozen immediately at -80°C to preserve the RNA until analyzed on RT-ddPCR.

Table 4. Components of custom Maxwell® HT Environmental TNA Kit (Promega, Catalog number AX9190).

Component	Description	Amount per kit
MC1411	CTAB Buffer, 100 mL	1
A176C	Wash Buffer (WBA), 350 mL	3
A2641	25 mM Tris-HCl, pH 8.0, 60 mL	2
A175B	Resin, 5.5 mL	4
AX918A	Alkaline Protease Solution, custom (APA), 60 mL	1
A173C	Cell Lysis Buffer (CLD), 160 mL	1

2.3 Comparison of Extraction Methods

2.3.1. Introduction

Wastewater Surveillance of COVID-19 in our laboratory has been part of the NWSS since August 2020 [48], but since then methods have evolved and improved to better detect and monitor SARS-CoV-2 [25]. In 2020, our lab began performing RNA extraction using an on-column silica membrane commercial kit procedure (Chapter 2.2.2-2.2.3)[46], however, studies have shown that magnetic bead approaches favor silica membrane approaches [49]. Methods used for RNA extraction tend to be the most important variable in determining the positivity of a sample for SARS-CoV-2, and even more so for laboratories lacking an automated nucleic acid extraction system [50]. So, in August 2021, our lab began experimenting using an automated magnetic-bead extraction procedure designed by the WI Department of Health Services (DHS). The purpose of Chapter 2.3 was to prove that adapting our protocol improved the sensitivity of

SARS-CoV-2 detection, especially in periods where there was a low prevalence of COVID-19 within the community.

2.3.2 Experimental Specific Methodology

To compare Qiagen and KingFisher extraction methods, 70 wastewater samples from July 16, 2021, to August 19, 2021, were filtered in duplicate, so that each sample could be extracted using both extraction methods. This analysis consisted of 152 total samples from 16 WWTPS in Wisconsin and North Carolina (Table 5). Samples were filtered, extracted, and processed according to methodology in Chapter 2.

Table 5. Wastewater treatment plants included in the Qiagen versus KingFisher analysis and how many samples from each WWTP was used in the analysis.

UWM WWTPs	Samples	DHS WWTPs[3]	Samples
BRK	7	Black River Falls	2
CED	6	Eau Claire	1
DP	7	Hayward	1
PLT	6	Madison-P18-NE	1
JI	7	Stevens Point	1
SS[1]	7	Stevens Point	1
Sylva[2],[3]	6	WI Rapids	1
RAC	7	Wolf	2
WAU	8		

[1] Sample from August 18th was ran five times to ensure reproductivity of both methods
[2] North Carolina WWTP processed biweekly by UWM
[3] Samples outside of biweekly UWM testing were not considered for full analysis

Sensitivity of each method was analyzed by comparing frequency of samples that were detected below LOD, below LOQ, and above LOQ for both N1 and N2 targets, in addition to the arithmetic average of N1N2 for all samples in Table 7. The N1N2 arithmetic average is what is used for DHS and CDC reporting [51]. Box plots and corresponding statistics were computed, and a Welch's t-test was performed to determine if the extraction method significantly impacts

SARS-CoV-2 concentration for only weekly-tested UWM samples indicated in Table 7. Nonparametric Kendall's tau was used to test if either extraction method had a better correlation between the sewershed-specific case rate and SARS-CoV-2 concentration detected from the wastewater sample for only weekly-tested UWM samples.

2.3.3 Results and Discussion

Extractions performed on the KingFisher detected significantly higher concentrations of SARS-CoV-2 compared to Qiagen (Welch's t-test, $p < 0.005$) in all WWTP's except SS (Figure 3).

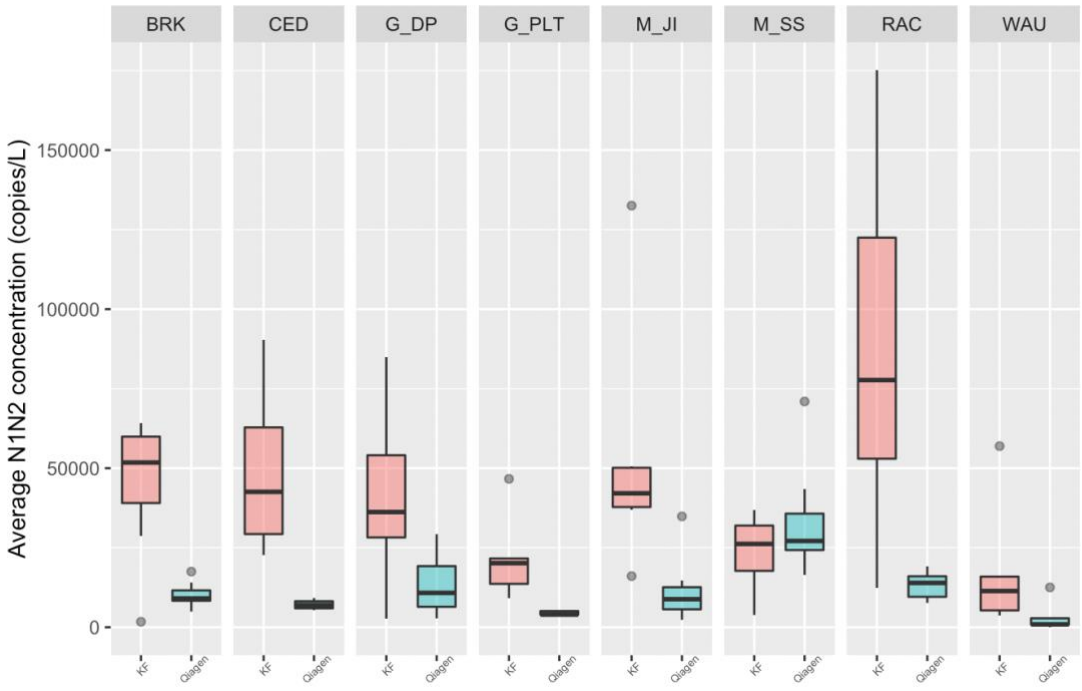

Figure 3. Box plot of the average N1N2 SARS-CoV-2 concentration in copies per liter for all samples above LOD from eight WWTPs from both KF (pink), and Qiagen (blue) extractions. The lower and upper hinges correspond to the 25th and 75th percentiles, the upper whisker extends from (1.5 * inter-quartile range (IQR)), the lower whisker extends from (1.5 * IQR) of the hinge, plots beyond the whiskers represent outliers, and the line in each box plot represents the median with a 95% confidence interval.

We later determined that SS was producing lower signals due to inhibition, so we began spiking half of the sample amount into the extraction (125 µL instead of 250 µL), and compensated the volume removed with pure isopropanol as indicated in Chapter 2.5. The total average concentration of all samples extracted via KingFisher increased concentration by 3-fold when comparing those extracted using Qiagen (Figure 4).

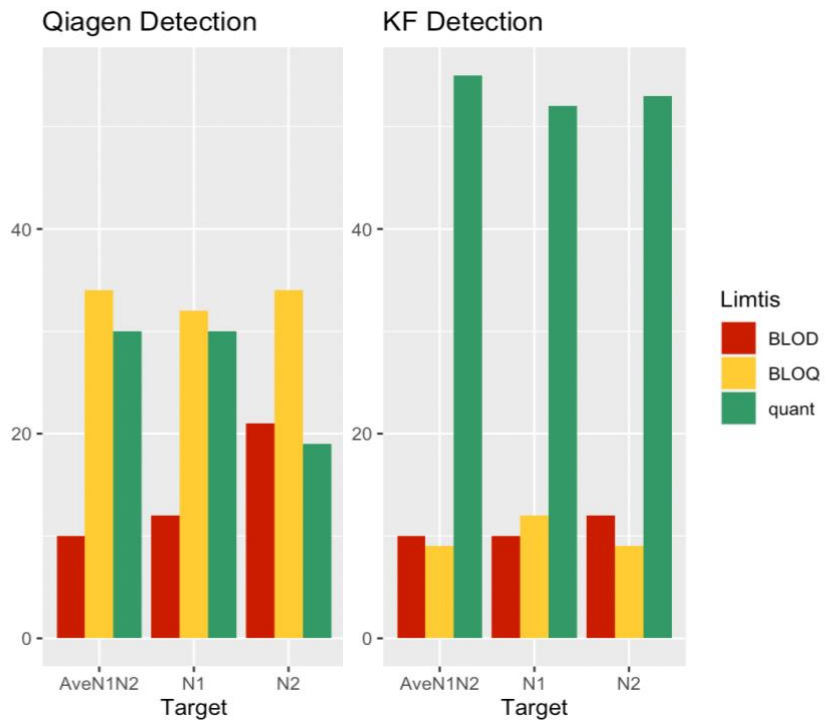

Limits	Value	Target	Extraction
BLOD	10	N1	KF
BLOD	12	N2	KF
BLOD	10	AveN1N2	KF
BLOQ	12	N1	KF
BLOQ	9	N2	KF
BLOQ	9	AveN1N2	KF
quant	52	N1	KF
quant	53	N2	KF
quant	55	AveN1N2	KF
BLOD	12	N1	Qiagen
BLOD	21	N2	Qiagen
BLOD	10	AveN1N2	Qiagen
BLOQ	32	N1	Qiagen
BLOQ	34	N2	Qiagen
BLOQ	34	AveN1N2	Qiagen
quant	30	N1	Qiagen
quant	19	N2	Qiagen
quant	30	AveN1N2	Qiagen

Figure 4. Number of extracted samples that are below the limit of detected (BLOD), below the limit of quantification (BLOQ), and above the limit of quantification (quant) from the Qiagen extraction (right graph), and KingFisher (left graph) represented in a bar graph (left), and data table (right).

This increase in concentration caused KingFisher extractions to fall above the LOD 74.3% of the time, while Qiagen samples were only above the LOD 40.5% of the time (Figure 4). This method change ensured a higher probability of detection when COVID-19 cases are low in the community. And, also improves the accuracy of quantification by increasing the number of

samples over LOQ, which is defined as the lowest concentration at which the analyte can be reliably detected [52].

Switching to the KingFisher did not significantly increase the correlation between the case rate to detection in the sewershed (Kendall's tau, $p = 0.88$), even with the removal of outlier SS (Kendall's tau, $p = 0.31$), within this dataset, but this could be for various reasons. These include, but are not limited to the small sample size used in this analysis, the fact that cases were relatively low during the period of this analysis, or that clinical testing data inaccurately reflected true incidences, such as asymptomatic cases going without testing [53]. When comparing the correlation of SARS-CoV-2 samples to clinical case rates in all KingFisher extracted samples from January 1, 2021, to January 30, 2022, there is a significant correlation (Kendall's tau, $p < 0.005$) (Figure 5).

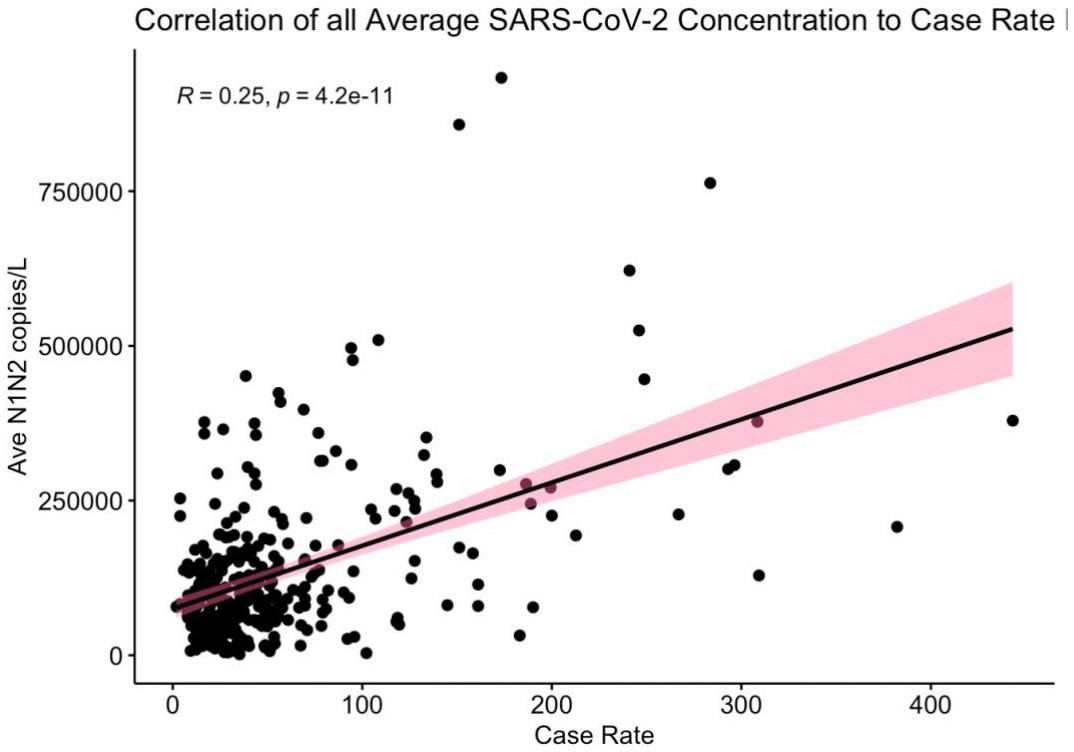

Figure 5. Kendall's empirical tau correlation on BRK, GB DP, GB PLT, JI, SS, RAC, and WAU on all samples extracted via KingFisher that were reported to WI DHS until January 30, 2022 (n = 414).

2.4 RT-ddPCR analysis

The SARS-CoV-2 reactions were set up following the One-Step RT-ddPCR Advanced Kit for Probes by Bio-Rad (Table 5) using primer and probe sets designed by the CDC to target the N1 and N2 regions of the SARS-CoV-2 N gene (Table 1). The primer's final concentration was approximately 900nM, and the probe's final concentration was approximately 250nM. All RT-ddPCR assays were performed in 22 μL reaction mixtures using the one-step RT-ddPCR Advanced Kit for Probes (Bio-Rad, Hercules, CA) with volumes as indicated in Table 5.

Table 6. Assay used for SARS-CoV-2 detection in wastewater influent and sludge on RT-ddCPR.

Reagents	**Volume per well (μL)**	**Final concentration**
Supermix	5.5	1X
RT	2.2	20 U/μL
DTT (300 nM)	1.1	15 mM
N1 Primers (18 uM each)	1.1	900 nM each
N1 Probe (5 uM)	1.1	250 nM
N2 Primers (18 uM each)	1.1	900 nM each
N2 Probe (5 uM)	1.1	250 nM
H2O	3.3	-
Sample	5.5	-
Total	22	

The RT-ddPCR assays were amplified using the Mastercycler pro (Eppendorf, Hamburg, Germany) with settings as indicated in Table 6. Reactions were not kept at 4°C for longer than 8 hours before being read using the Bio-Rad QX200 Droplet Digital System (BioRad, CA). Each sample was run individually unless indication of the need for a rerun as described in Chapter 2.5.4. Raw droplet amplification data was extracted from the Bio-Rad QuantaSoft Analysis software and processed using R package twoddpcr (version 1.11.0) in R-Studio (version 1.4.1103).

Table 7. Mastercycler amplification settings.

Assay	Step	Cycle #	Temp °C	Time (min)
N1 N2 BCoV BRSV	Reverse Transcription	1	50	60
	Enzyme Activation	1	95	10
	Denaturing	40	94	0.5
	Annealing/Extension	40	55	1
	Enzyme Deactivation	1	98	10
	Droplet Stabilization	1	4	30
PMMoV	Reverse Transcription	1	50	60
	Enzyme Activation	1	95	10
	Denaturing	40	94	0.5
	Annealing/Extension	40	60	1
	Enzyme Deactivation	1	98	10
	Droplet Stabilization	1	4	30

2.5 Processing Controls

2.5.1 Recovery Controls

Bovine Coronavirus (BCoV) was spiked into each sample prior to filtration to act as a recovery estimate for each filtration. The BCoV used was the Calf Guard cattle vaccine (Zoetis, Parsippany, NJ) rehydrated with 3 mL of 1x TE buffer so that the final concentration per sample is about 100,000 cp/µL for influent and for sludge samples. To define the concentration of the hydrated BCoV stock solution, raw BCoV was extracted using the same protocol as the influent or sludge then serially diluted 1:2 for four dilutions and run in duplicate using the BCoV assay [1] according to the one-step RT-ddPCR. BCoV recovery (R_{BCoV}) was calculated as a ratio of this value using the equations 1 and 2 in R-studio:

$$R_{BCoV} = \frac{C_{obs}}{C_{exp}} \times 100 \quad (1)$$

$$C_{exp} = \frac{V_R * C_{BCoV}}{V_S} \times 1000 \quad (2)$$

Where C_{obs} is the BCoV concentration in copies per liter of sewage detected in each individual sample ran on ddPCR, and C_{exp} is the expected BCoV concentration in copies per liter of sewage obtained as indicated in section 2.4.1. (V_R) is the volume in uL of raw BCoV spiked into solution, (C_{BCoV},) is the concentration per uL of BCoV solution detected by the RT-ddPCR reaction, and V_S is the total sample volume in uL processed.

2.5.2 Fecal Strength Indicators

The fecal strength of untreated wastewater was determined by quantifying the human marker, PMMoV, in each sample [31]. A 1:10 dilution of each sample was made if extracted using the Qiagen Kit, a 1:40 dilution of each sample was made if extracted via KingFisher. An assay was performed according to the one-step RT-ddPCR procedure as described in Chapter 2.4.

2.5.3 Inhibition Controls

The effects of untreated wastewater samples on RT-ddPCR amplifications of SARS-CoV-2 were determined by comparing Bovine Respiratory Syncytial Virus (BRSV) prepared from 25 doses of freeze-dried Inforce 3 Cattle Vaccine (Zoetis, Kalamazoo, MI, USA). Inhibition was evaluated in each sample by spiking approximately 4000 copies of BRSV into each RT-ddPCR reaction and comparing the concentration of each well to two reference wells containing deionized water spiked with the same amount of BRSV made on the same plate. If the ratio of any reaction to either of the reference wells was within 50%, it concluded that the wastewater matrices had negligible inhibitory effects on the detection of SARS-CoV-2 RNA [46], [54].

2.5.4 Additional Quality Control

For all RT-ddPCR assays, two no-template controls (NTC) using nuclease-free water were run to ensure no contamination occurred. Each run was analyzed only if both NTCs per assay were below the limit of detection (LOD), which was assigned as 3 droplets (~0.2209 copies/uL). If either NTC was above the LOD, the entire assay was rerun. For the N1/N2 duplex assay, duplicate 1:8 diluted Exact Diagnostics SARS- CoV-2 standard (Bio-Rad) wells were used in each run as a standard control. Both standards were confirmed to be approximately 100 droplets prior to processing the plate. See Feng et. al. for further in-depth description of processing controls and determination of LOD and limit of quantification (LOQ) [46].

2.6 Data analysis

All data compilation and statistical analysis were performed in R-Studio version 1.4.1103 [55]. All samples used for analysis are above the LOD, and none exhibited inhibition. Specific statistical tests utilized for each experiment are explained within that chapter under "Experimental Specific Methodology."

Chapter 3. Wastewater surveillance using RT-ddPCR accurately tracked Omicron emergence due to altered N1 probe binding efficiency

3.1 Introduction

A portion of this chapter was previously published as a preprint by medRxiv [56] and is currently undergoing peer review for publication in Environmental Science: Water Research & Technology.

Mutations of the COVID-19 virus in the form of variants have also caused pressured adaptations of laboratory methodology. The Omicron variant is unique in that it contains a high number of mutations that appeared sporadically with the nearest ancestral strain last documented in the community almost a year previously [57]. While most mutations accumulate in the spike protein, Omicron also contains a mutation in the N gene that corresponds to the N1 probe binding site of the CDC assay [58]. RT-ddPCR platforms provide data for individual molecules and can reveal a decreased but positive fluorescence intensity in discrete reactions. One study reported the Omicron mutation in the N1 probe of the CDC assay did not perturb N1 detection but did note a slightly reduced cycle threshold (Ct) value for the N1 target [59]. The purpose of Chapter 3 was to illustrate how RT-ddPCR may be a preferred platform for wastewater surveillance since it was able to accurately track the Omicron variant emergence and fixation due to the diminished fluorescence signal in the CDC N1 assay.

3.2 Experimental Specific Methodology

We quantified SARS-CoV-2 N-gene, Delta variant, and Omicron variant concentrations in influent samples in five communities as part of our ongoing WI SARS-CoV-2 wastewater

surveillance program [51]. SARS-CoV-2 concentration and variant analysis for this paper includes a total of 165 samples that were collected between November 14, 2021, and January 31, 2022. Samples were collected from seven WWTPs: BRK, DP, PLT, JI, SS, ORE, and RAC. Samples were collected and processed according to Chapter 2. In addition to the RT-ddPCR assay primers probes indicated in Chapter 2, mutation assays for the Delta and Omicron variants used in this experiment (Applied Biosystems, Waltham, Massachusetts, USA) are shown in Table 8.

Table 8. TaqMan SARS-CoV-2 Mutation Assays used for RT-ddPCR variant analysis. *

Target	Primer/Probe Sequence (5'-3')[a]	Supplier	Ref
Delta (P681R)	Reporter 1 dye: VIC, Reporter 1 Quencher: NFQ, Reporter 2 dye: FAM, Reporter 2 quencher: NFQ CTCAGACTAATTCTC[C/A]TCGGCGGGCACGTAG	Applied Biosystems	[60]
Omicron (P681H)	Reporter 1 dye: VIC, Reporter 1 Quencher: NFQ, Reporter 2 dye: FAM, Reporter 2 quencher: NFQ, CTCAGACTAATTCTC[C/G]TCGGCGGGCACGTAG	Applied Biosystems	[60]

*RT-ddPCR primers and probes at a final concentration of 900 nM and 250 nM, respectively.
[a]Reporter 2 dye targets Mutant of TaqMan SARS-CoV-2 Mutation Panels.

Detection of the Omicron variant was derived from RT-ddPCR droplet data, which was processed using the QuantaSoft Software, version 1.7, for the Bio-Rad QX200 Droplet Digital System (Bio-Rad, Hercules, CA). Raw droplet amplification of the Omicron variant in each sample was assigned using the lasso threshold adjustment tool to reclassify the cluster delineation in the 2D amplitude scatterplots. To ensure the correct amplitude was being associated with each respective variant, we included an Omicron and Delta residual clinical sample diluted 1:100 in addition to two 1:8 diluted Exact Diagnostics SARS- CoV-2 standards (Bio-Rad). Raw droplet amplification data for each variant and total N1 and N2 gene concentration were extracted from the Bio-Rad QuantaSoft software and processed using R package twoddPCR according to Chapter 2.

To validate the observed diminished fluorescence corresponding to a mismatch at the 5'end of the N1 probe, we mimicked the same type of substitution in an artificial N2 template. We synthesized a 300-basepair template that contained an A:C change in the third nucleotide position of the N2 probe binding site (Twist Bioscience, South San Francisco, California, USA). We tested this template in RT-ddPCR using increasing ratios of the SARS-CoV-2 standard and of Omicron and Delta residual clinical samples and analyzed droplets as described above.

3.3 Results and Discussion

Throughout late November through December 2021, we found that SARS-CoV-2 levels steadily increased and the N1 signal in RT-ddPCR could be separated into two distinct clusters, one with lower fluorescence than expected based on the N1 standard (Figure 6). The Omicron variant has a C to U mutation at position 28,311 in the SARS-CoV-2 genome, which corresponds to the nucleotide position on the 5' end of the probe for the CDC N1 PCR assay [28]. The loss of fluorescent signal is likely due to inefficient exonuclease activity of the Taq polymerase on the 5' end of the probe which releases the fluorophore from the quencher.

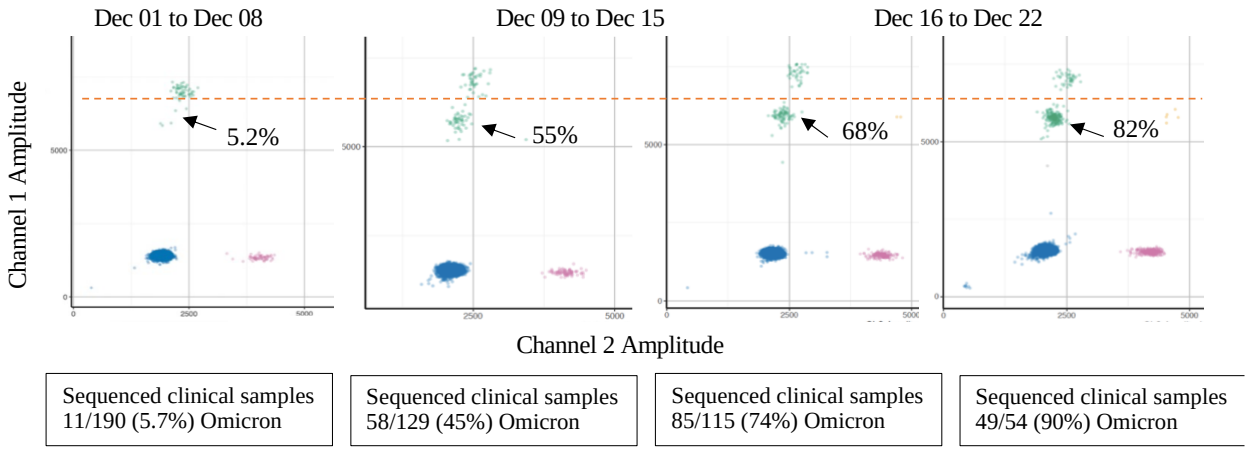

Figure 6. Wastewater N1N2 multiplex RT-ddPCR results in JI throughout December 2021 during the Omicron variant surge. A reduced fluorescence in the N1 signal in Channel 1 (green droplets) resulted in two clouds and was indicative of Omicron. N2 signal is in Channel 2 (pink droplets). Channel 1 and 2 fluorescence in the same droplet indicate both N1 and N2 target are present (yellow droplets) Negative droplets are blue. Clinical patient samples sequenced from Milwaukee County each week are indicated below graph (data from GISAID).

We verified the loss of fluorescence due to the C to U mutation by synthesizing a DNA template containing a similar nucleotide change in 5' end of the N2 probe binding region. The third position of the N2 probe was substituted (A:C). We found fluorescence diminished similar to what was observed in the Omicron variant (Figure 7). The effects of probe mismatches on fluorescent signal have been previously reported [61]. The probe is impacted more by mutations nearer the 5' end, in contrast to primers, where mismatches in the 3' end are more likely to affect the extension activity of the polymerase [62]. Overall, mutations in the probe rather than the primers are more likely to result in reduced quantification [63].

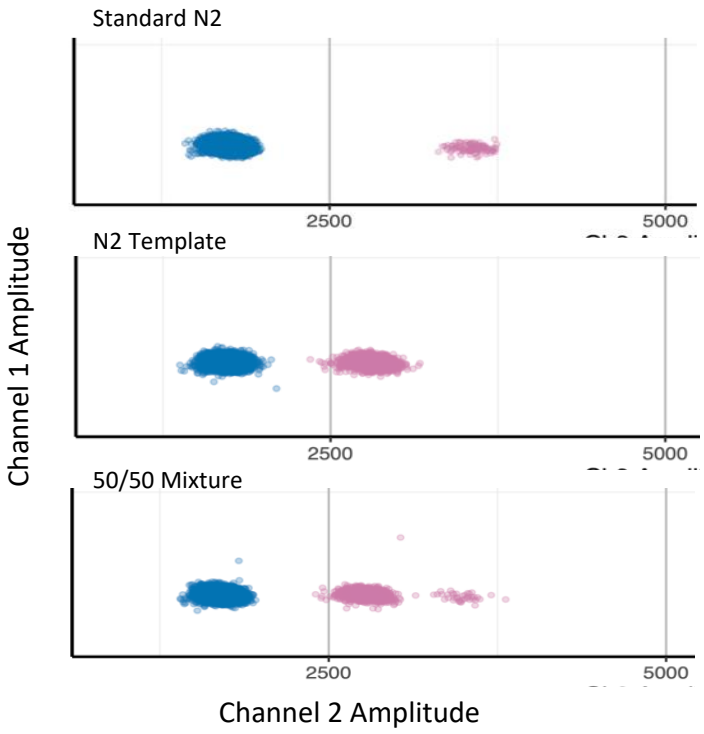

Figure 7. N2 multiplex ddPCR results of 1:8 diluted Exact Diagnostics SARS- CoV-2 standards (Bio-Rad) (top image), 1:100000 diluted (1 ng/uL) 300bp linear synthesized DNA N2 sequence with A:C mutation on the third base pair (Twist Bioscience) (middle image), and a 50/50 mixture of both samples (bottom image). Channel 1 amplitude above baseline (i.e., N1 signal, not shown).

We validated the accuracy of quantifying the Omicron variant using the N1 cloud splits with the TaqMan SARS-CoV-2 Mutation Panels S.P681R.CCT.CGT (Delta) and S.P681H.CCT.CAT (Omicron) (ThermoFisher Scientific, Waltham, MA) in two WWTPs. A significant positive correlation was observed between the specific mutation assay and N1 cloud split quantification for Omicron (Spearman's rank correlation, rho = 0.845, $p < 0.005$) and Delta variants (Spearman's rank correlation, rho = 0.785, $p < 0.005$). The trends in the variant concentrations mirrored each other (Figure 8), but overall, the N1 assay was more efficient (i.e. higher number of droplets) than the specific mutation assays.

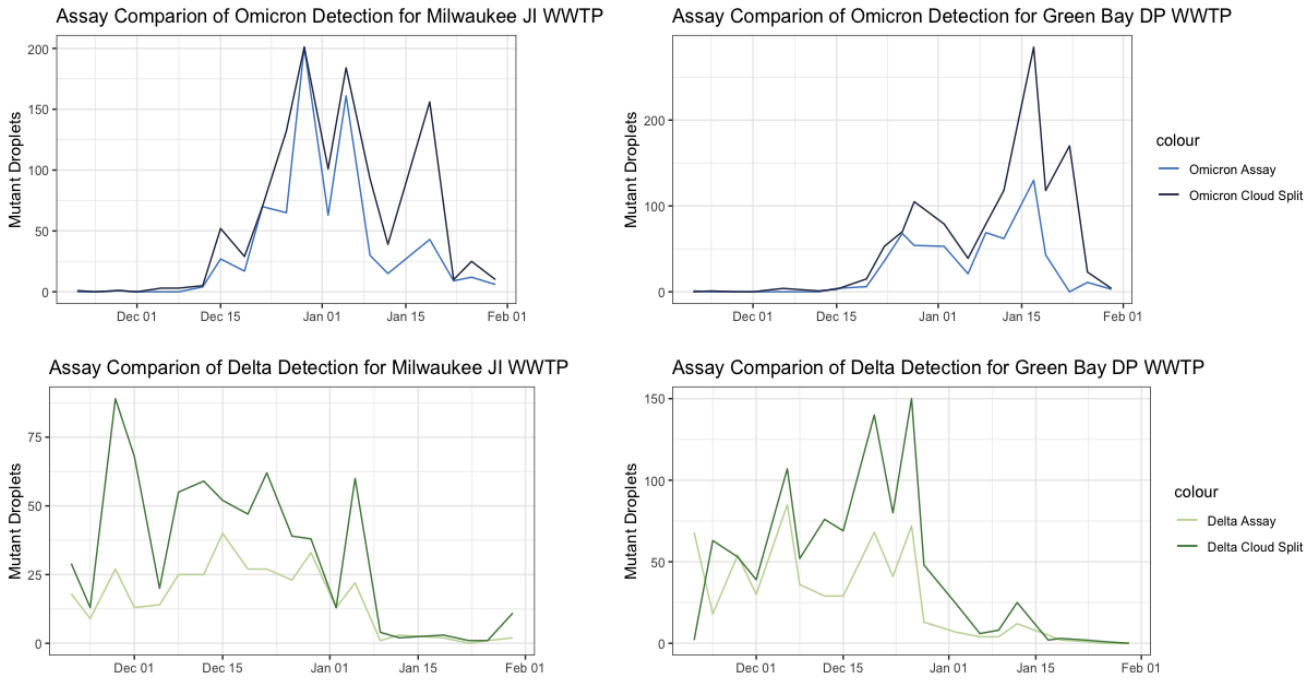

Figure 8. Comparison of the quantification of Omicron and Delta mutant droplets using the TaqMan SARS-CoV-2 Mutation panels and N1 probe cloud split methods.

We also compared the proportion of Omicron and Delta in wastewater with sequencing results from clinical samples available in GISAID [64] for the communities serviced by seven WWTPs (Figure 9). We assumed that county-level data would be a proxy for different cities

within the county. There was good agreement between WWTPs within the same city or county, and in all cases, the WWTP serving the larger population detected omicron earlier.

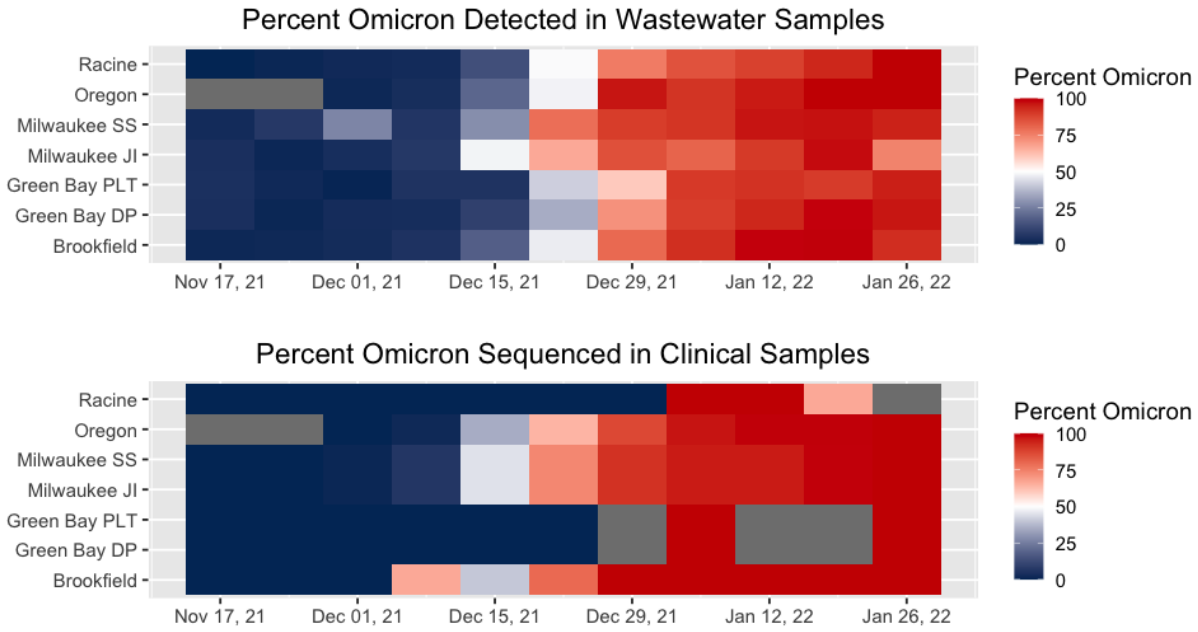

Figure 9. Heat map of percentage of Omicron in (a) WWTP samples determined by RT-ddPCR and (b) clinical samples determined by sequencing as reported in GISAID. In general, the WWTP samples showed a more gradual progression. Gray bars indicate no clinical samples were sequenced in the counties in which those cities are located.

In all WWTPs, Omicron was detected greater than the LOD prior to the first clinically confirmed case of Omicron (Table 9). Our first sample indicating a second N1 cluster above the LOD was a sample from November 21, 2021, one day prior to the first diagnosed clinical Omicron sample in the US. This date is identical to east and west coast wastewater detection [65], but is noteworthy as variants of concern are not usually first observed in Midwest states.

Table 9. Dates of first detection of Omicron by whole genome sequencing of clinical samples and routine analysis of RT-ddPCR of wastewater samples.

WWTP	County	First clinical	First >LOD wastewater	Days from first >LOD to 75% Omicron	Population
Racine	Racine	5-Jan-22	5-Dec-21	28	139000
Oregon	Dane	12-Dec-21	8-Dec-21	29	10000
Milwaukee SS	Milwaukee	1-Dec-21	21-Nov-21	35	615934
Milwaukee JI	Milwaukee	1-Dec-21	5-Dec-21*	21	470007
Green Bay PLT	Brown	30-Dec-21	28-Nov-21	39	189000
Green Bay DP	Brown	30-Dec-21	6-Dec-21	27	43000
Brookfield	Waukesha	7-Dec-21	28-Nov-21	30	51000

*Milwaukee JI 17-Nov-21 sample was run in two RT-ddPCR wells to increase sensitivity and found to be >LOD.

When comparing our wastewater data to sequenced clinical samples, we saw a later onset of Omicron in clinical samples, with a more rapid spike in percentage. In addition, there were various instances where no clinical samples were sequenced for that county. The low number of clinical samples sequenced for less populated parts of the state might not accurately portray proportions. For example, 21 clinical samples were sequenced in Racine County and 23 in Brown County for the entire month of December. Because clinical sequencing may not be equally resourced across a state, the results of wastewater testing are expected to be more consistent. Further, sequencing of clinical samples might be biased toward testing for variants in samples from vaccinated individuals or in samples with S gene target failure, which can be an indicator of specific variants [66].

We further examined wastewater dynamics through the pandemic and found the emergence and shift to dominance of the Alpha, Delta, and Omicron variants was characterized by increasing percentages in wastewater over increasingly shorter time frames (12 weeks, 7 weeks, and 2-4 weeks, respectively) (Figure 10). For each variant shift, the total abundance of

viral signal in wastewater reached higher levels than previous surges. Clinical testing has changed dramatically over the pandemic, however, we found wastewater pattern mirrors the dynamics captured with traditional clinical testing and sequencing [67].

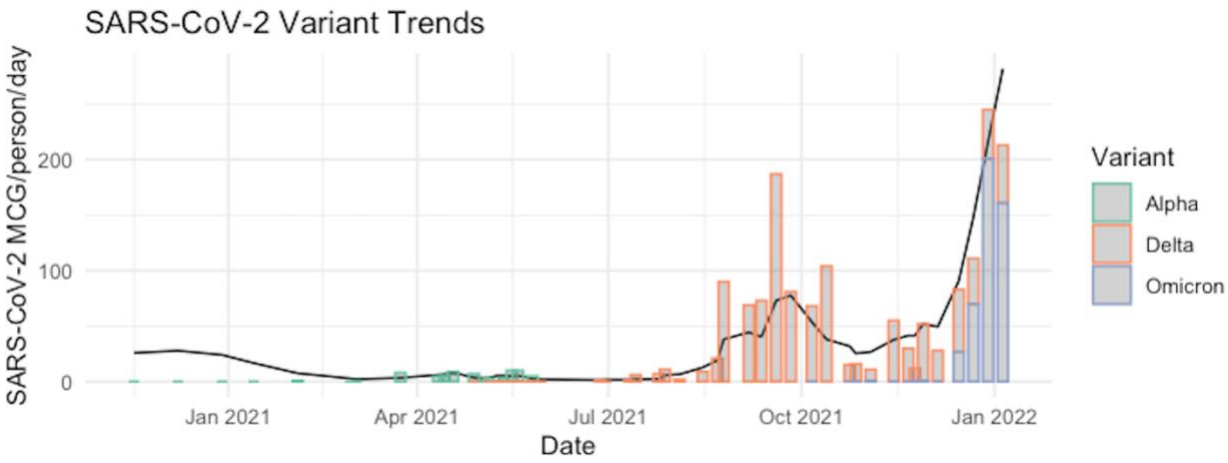

Figure 10. SARS-CoV-2 levels determined by averaged N1 and N2 levels in wastewater during four surge periods and the level of each variant. Alpha variant became dominant (>50%) in 12 weeks, Delta in 7 weeks, and Omicron became dominant in 10 days, with the highest N1N2 levels ever seen in wastewater. The increase in the variants preceded the increase in overall N1N2 concentrations.

Chapter 4. Effect of Wastewater Matrix on SARS-CoV-2 in Municipal Wastewater Conveyance Systems

4.1 Introduction

A section of this chapter has been published by Water [68]. The goals of this chapter were to obtain an accurate residence time of two sewer networks to examine travel time effects on decay and to determine how wastewater parameters may affect SARS-CoV-2 RNA concentrations entering wastewater treatment plants (WWTPs). Because SARS-CoV-2 is an enveloped positive-sense single-stranded RNA virus [69] its outer lipid layer may render it more sensitive than other viruses to temperature, organic solvents, and other constituents encountered in the wastewater conveyance system [70]. While various studies have performed analysis on the decay of coronaviruses, and specifically SARS-CoV-2 RNA in wastewater influent in a laboratory setting, they are often done with surrogate SARS-CoV-2 RNA spikes [43], [71]–[74] which have been shown to behave differently than authentic in-situ SARS-CoV-2 found within the wastewater matrix [75], [76]. A major barrier to performing in-situ studies and comparing across real wastewater systems is that the true input of SARS-CoV-2 virus from the population is unknown and likely different for individuals depending on the severity of disease, stage of infection, and other factors [34].

This study utilized two wastewater service areas, with one surrounded by a second large one, that service a single large metropolitan area. The similar case rates and close geographic proximity allowed us to analyze how various parameters can affect SARS-CoV-2 concentration during the residence time within each sewer network. In this study, the approximate travel time at different flow rates (average, maximum, and minimum) for two service areas were

determined. The two conveyance systems have different travel times, which we used to assess the loss of SARS-CoV-2 signal during longer travel times. We also examined the effect of flow rate, temperature, BOD, and TSS on SARS-CoV-2 (N1 and N2 targets) in both WWTPs. Additionally, to gain insight into dilution effects, we analyzed the flow rate, and human fecal (PMMoV) concentration. It was determined that within typical residence times (up to 100 hours) of SARS-CoV-2 within the wastewater matrix, temperature was the only parameter that had a significant influence on SARS-CoV-2 concentrations.

4.2 Experimental Specific Methodology

4.2.1 Study Area and Engineered Parameters

The Milwaukee Metropolitan Sewage District (MMSD) is comprised of two separate WWTPs; JI which serves a population of 470,007 residents, and SS which serves a population of 615,934 residents in Milwaukee County, Wisconsin, USA (Figure 11). A portion of JI (37%) services a combined sewer system, meaning that industrial, urban, residential, and environmental run-off all contribute unique factors to the wastewater matrix. SS serves a much larger area, and its sewer network is better equipped for larger flows (average pipe diameter SS = 43.6 inches, average divertible pipe diameter from JI = 32.8 inches). Under high flow conditions, 47% of JI sewers can be diverted to SS (Figure 11) to avoid sewer back-ups. This diversion only increases the SS sewer network by 11%. Overall, the SS conveyance system is comprised of a larger surface area and has longer travel times.

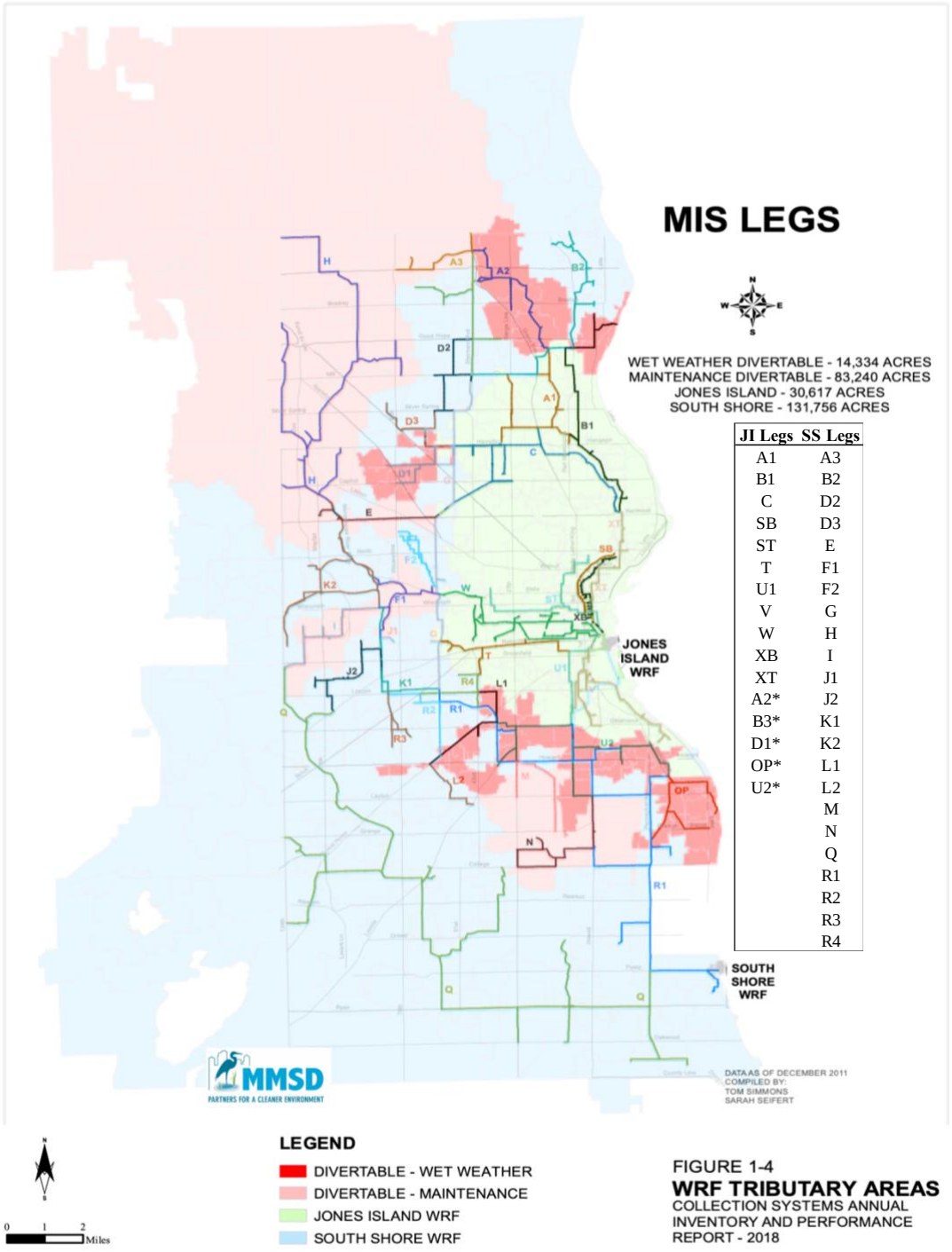

JI Legs	SS Legs
A1	A3
B1	B2
C	D2
SB	D3
ST	E
T	F1
U1	F2
V	G
W	H
XB	I
XT	J1
A2*	J2
B3*	K1
D1*	K2
OP*	L1
U2*	L2
	M
	N
	Q
	R1
	R2
	R3
	R4

Figure 11. MMSD sewer tributary areas consisting of 162,373 acres of land divided between JI and SS sewer systems. Collectively 131,756 acres goes to SS WWTP (blue), and 30,617 acres goes to JI WWTP (green). 14,334 acres of JI service area can be diverted to SS under high flow conditions (dark red). Divertible maintenance pipes are indicated by light red. The legend indicates which legs (labeled on map) flow to which WWTP. Legs with an * indicate legs that are diverted to SS under high flow conditions, this area makes up 11% of the SS service area. Map provided by MMSD.

4.2.2. Sampling

Our analysis included a total of 186 samples that were collected biweekly between August 26, 2020, to August 22, 2021, from JI and SS WWTPs that were collected and processed as indicated in Chapter 2. The average parameter values confirmed that both conveyance systems had similar conditions except for biological oxygen demand (BOD) (Table 10).

Table 10. Comparison of JI and SS parameters across all samples (n=186), and in warmest (n=70) versus coldest (n=38) months. Samples are collected from an automated samplers at MMSD reclamation facility, aliquots are removed by WWTP operators.

Parameter[a]	**SS Average**	**JI Average**
Warmest temperatures (°C)	17.86	18.54
Coldest temperatures (°C)	10.97	10.35
Annual temperature (°C)	14.9	15.30
Warmest Daily Average Flow Rate (MGD)	82.29	89.69
Coldest Daily Average Flow Rate (MGD)	92.58	86.32
Annual daily average flow rate (MGD)	79.00	83.30
Warmest TSS (mg/L)	267.71	247.69
Coldest TSS (mg/L)	253.16	233.16
Annual TSS (mg/L)	273.00	245.00
Warmest BOD (mg/L)	331.43*	271.40
Coldest BOD (mg/L)	314.74	248.95
Annual BOD (mg/L)	343.00*	273.00

[a]Total suspended solids indicated as TSS
*Significantly different values

4.2.3. Travel Time Calculation

The MMSD sewer system is a complex network containing 39 separate legs of large pipes comprising a municipal interceptor system that eventually flow to either JI or SS WWTP. Each leg was assigned a different letter or letter combination (Figure 11). The approximate minimum, maximum, and average travel times were calculated for both JI and SS using equation 3.

$$T_h = \frac{\left(\frac{L}{B}\right)}{V} \quad (3)$$

Where the travel time in hours in hours (T_h) is equal to the total leg length in meters (L), divided by the number of branches within a leg that lead to the same outfall (B), divided by the metered velocity in meters per second (V), which was measured hourly. A total of 56.5% of the velocity values fell below the average and 43.5% above the average.

MMSD provided hourly velocity data captured from individual meters throughout 33 of the 39 legs, excluding B1, R4, ST, U1, XB, and XT, for the entire timeline of our sample collection. Additional information used to complete the calculation included the location of each meter within the treatment system, the length, diameter, and slope of each pipe, the inlet and outlet pipes of each leg, and the direction of flow. Velocity from four representative subsewersheds in SS and three representative subsewersheds in JI are displayed in Figure 12.

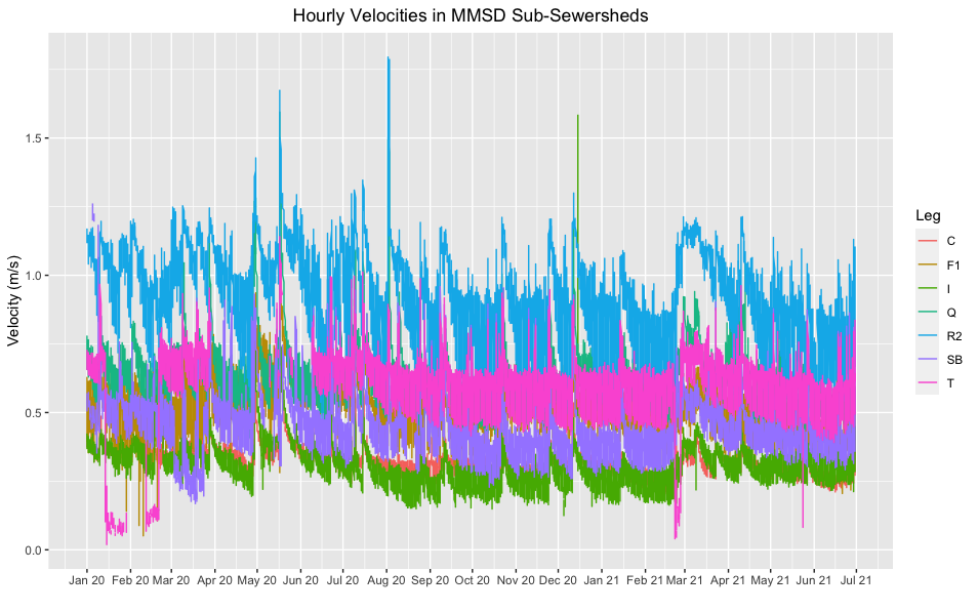

Figure 12. All positive hourly metered velocity readings from four representative subsewersheds in SS WWTP (within legs Q, R2, SB, T), and three representative subsewersheds in JI WWTP (within legs C, F1, I) over the course of this study.

Various instances of negative velocity values were collected at each meter, which indicates the sensor was not measuring accurately at that time. This could have resulted from a variety of issues including fouling, debris, equipment failure, poor flow conditions, or levels below necessary minimums. For this analysis, all negative values were removed from the dataset. Using only the positive values from the 13,128 hourly readings for each meter between January 1, 2020, to July 1, 2021, the minimum, maximum, and average velocities were calculated in R-Studio for each metered section. For the six legs mentioned above that were not metered, approximate velocity values were estimated using an average of the most similar pipes according to slope, length, diameter, and location (Table 11).

Table 11. Estimated travel times using approximation of most similar legs. All legs used for this analysis were in urban areas. The average slope and average diameter are both listen in inches.

Leg	Slope	Diameter (in.)	Matched to	Slope	Diameter (in.)
B1	0.004	41	R2	0.004	43
ST	0.007	50	D3	0.006	44
U1	0.001	36	U1	0.001	34
XB	0.014	27	SB	0.019	33
XT	0.005	61	Q	0.004	46
R4	0.006	48	R2	0.004	43

To avoid unattainably high or low travel times the absolute minimum and maximum velocities of each leg were not used. Rather, to simulate high-flow travel times metered measurements from the highest summed velocity readings from each leg was used. The time for this collection window was May 17, 2020, at 16:00. To simulate low-flow travel times, the date of the lowest sum of total velocity measurements was applied to each leg of the conveyance system. November 23, 2020, at 4:00 provided the lowest hourly velocity readings. Leg G had no measured metered velocity on May 17th, so the absolute maximum velocity of that leg (0.637 m/s) was used.

The absolute minimum velocity of each leg was used where negative velocity readings were collected due to levels being too low for accurate meter readings. Out of the entire data set, minimum values were supplemented for leg D2 (0.365 m/s), leg E (0.015 m/s/), leg M (0.021 m/s), leg N (0.015 m/s), and leg V (0.055 m/s). For the average travel time estimate, the arithmetic average velocity for each meter was used. While the sewer system is designed to divert an additional 10% of acreage to SS under severe high-flow conditions, diversions were not considered because they are rare events. Further, flows to each respective WWTP during diversions only minimally affects travel times (Supplemental Table 12).

4.2.4. Temperature Analysis

The temperature analysis was done using hourly metered temperature data from four representative subsewersheds in SS and three representative subsewersheds in JI provided by MMSD (Figure 13). Daily temperature was calculated for each sample collection date summing the arithmetic average temperature for each meter respective to SS and JI sewersheds. Over the course of the year, the lowest recoded temperature was 6.05°C and the warmest was 21.73°C. To compare how much of an effect temperature had on SARS-CoV-2 case adjusted concentration, we compared data from the warmest (August, September, October), and coldest (February, March, April) months.

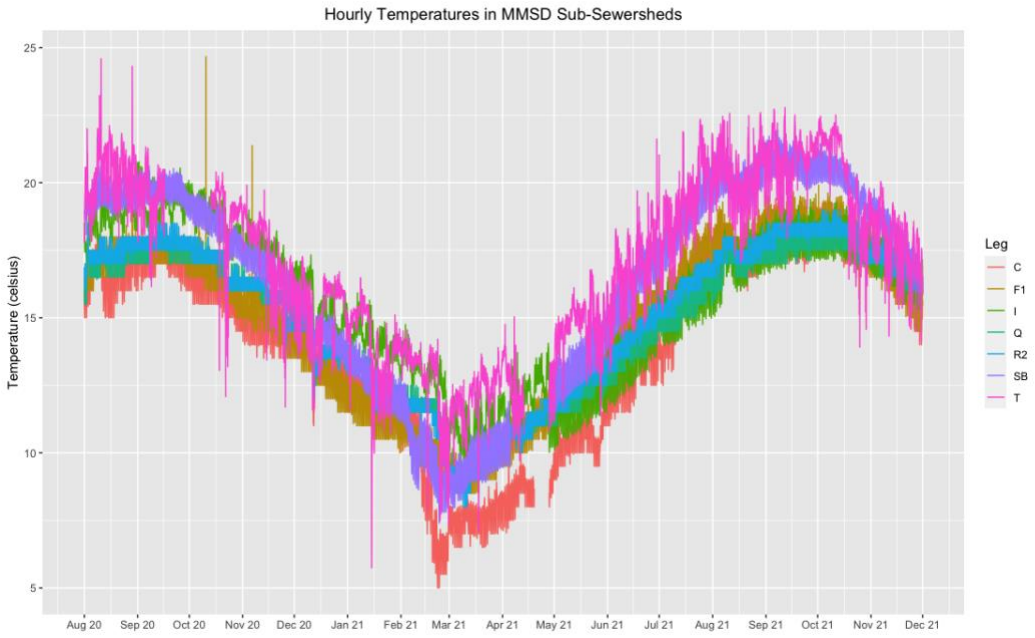

Figure 13. Hourly metered temperature readings from four representative subsewersheds in SS WWTP (within legs Q, R2, SB, T), and three representative subsewersheds in JI WWTP (within legs C, F1, I) over the course of this study.

4.2.5. Time and Temperature Analysis

After determining JI has a shorter travel time than SS, we hypothesized that SARS-CoV-2 copies per diagnosed case should be equal for the two service areas if travel time did not affect measured concentrations. We assumed that the amount of case under-reporting would be similar for the two populations. We confirmed that the case rate was equal in both sewersheds (Paired t-test, p = 0.81), supporting our assumption. The difference in copies per case would reflect the influences of the conveyance system environment such as effects of temperature, or decay during longer travel time.

To normalize between JI and SS service areas, quantified RT-ddPCR SARS-CoV-2 RNA concentrations were expressed as copies per case per day (C_p) using the equation 4.

$$C_p = \frac{(C \times Q)}{R} \tag{4}$$

Where *C* is SARS-CoV-2 RNA copies (in millions) per liter of wastewater, *Q* is the flow of the sewershed (in million liters per day), and *R* is the number of reported clinical cases (day of collection) on the day of wastewater sampling. All clinical data was obtained from Office of Health Informatics and the Bureau of In-formation Technology Services at the Wisconsin DHS and is reported as date of sample collection. Date of clinical sample result from each WWTP service area can be downloaded from https://www.dhs.wisconsin.gov/covid-19/wastewater.htm#wastewater. When determining how flow diluted the signal, flow was removed from this equation, resulting in SARS-CoV-2 concentration (C_f) being calculated using equation 5.

$$C_f = \frac{C}{R} \tag{5}$$

4.2.6. Statistical Analysis

Nonparametric Kendall's tau was used to test hypotheses' regarding correlations between variables and SARS-CoV-2 copies per case, and t-tests were used to test hypotheses regarding relationships and trends with the data. Comparing two interrelated WWTPs; one with a long travel time (up to 109 hours), and one with a short travel time (as low as 4 hours), we used a paired t-test to determine if time impacts SARS-CoV-2 copies per case within the wastewater conyence system.

Welch's t-test was used to analyze how each parameter (temperature, flow, BOD, TSS) impacts SARS-CoV-2 copies per case. We further examined the temperature data for significant outliers using a one-way analysis of variance (ANOVA), and posthoc Tukey Honestly Significant Difference (HSD) analysis in R-Studio to compare each month within the warm (August,

September, October) versus cold months (February, March, April) data sets. We further analyzed how much flow can dilute the fecal matter in the wastewater using Kendall's rank coefficient to compare human fecal marker PMMoV, and average daily flow rate.

4.3 Results

4.3.1. Travel time determinations and influences on SARS-CoV-2 decay

The average travel time for SS was approximately 3 times longer than JI (Table 12), and the ratio scaled similarly when comparing high and low flow conditions. Using velocity measurements from May 17, 2020, to simulate high flow conditions, SS transit was approximately 2.75 times longer than JI. And when using the minimum velocity to simulate low-flow conditions, the difference in travel time rose to almost 6 times longer. The simulated low-flow travel times (using the minimum velocity) within a WWTP lengthen the average residence time in the sewer network up to 5 times longer than high-flow conditions simulated with maximum velocity.

Table 12. Average, and simulated low-flow (maximum), and high-flow (minimum) travel times in hours in JI and SS WWTPs. The data was compiled using the length of each pipe, and the average velocity from 33 metered sites across 39 legs in the MMSD sewer network.

WWTP	Minimum Travel Time* (h)	Average Travel Time (h)	Maximum Travel Time (h)
JI	4.68	7.45	11.36
SS	12.88	22.16	63.45

*Minimum travel time with diversions is estimated to be 5.25 hours for JI and 13.17 hours for SS as indicated in Supplemental Figure 2.

In general, travel time had little effect on SARS-CoV-2 concentrations entering the WWTP. An increase from approximately 7.5 to 22 hours only resulted in a 10% decrease in average copies per case when comparing JI and SS travel times. Further, estimated decay rates are negligible (Appendix 2). While there was not a significant difference in the SARS-CoV-2 copies per case detected from the WWTPs, there was a trend shifting towards significance (paired t-test, $t=1.741$, $p = 0.08$) indicating that while there is minimal difference in decay within the first ~24 hours of travel time, significance may increase if the travel time increases. We further examined the difference in the SARS-CoV-2 copies per case (i.e., case-adjusted loads) under high-flow and low-flow conditions by using the maxmium and minimum third of daily average flow rates (Figure 14). We expected under high flow conditions, there would be no difference in copies per case between the WWTPs since travel time differs by only ~8 hours, which was confirmed by our analysis (Figure 14). When simulating low-flow conditions by considering minimum flow in all legs, there is up to an ~80-hour difference in travel time; however, we also did not observe a difference in JI vs. SS case-adjusted loads between, suggesting that the SARS-CoV-2 signal is not affected by travel time.

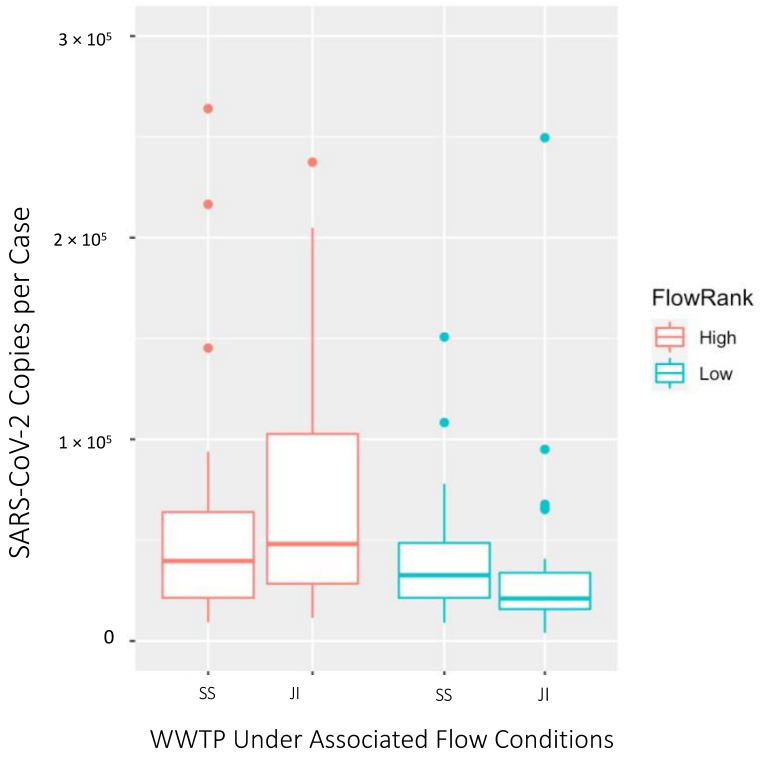

Figure 14. Case-adjusted loads (daily) among the highest and lowest third of average daily flow rates from 62 pairs of samples from JI and SS WWTPs.

4.3.2. Influence of flow

We investigated how flow might affect concentrations beyond the effect of the shorter travel times. Therefore, we examined if higher flows had a proportional reduction (i.e., dilution) on case-adjusted concentrations and of PMMoV. PMMoV is a human fecal marker that is widely present in the human population, that acts as a measure of fecal contribution. SARS-CoV-2 case-adjusted concentrations were on average 50% higher in high flows compared to low flows in JI (Welch's t-test, $p = 0.01$). This might be suggestive of the addition of SARS-CoV-2 due to scouring

with high velocities, as opposed to a dilution effect. SS case-adjusted concentrations were slightly higher with high flows, but this was not significant (Welch's t-test, p = 0.14) (Figure 15).

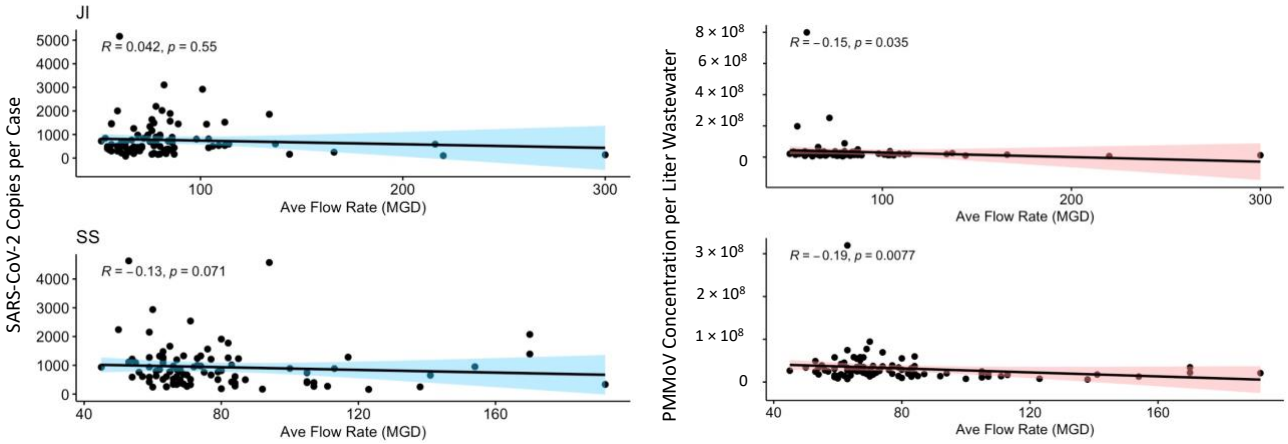

Figure 15. Kendall's rank correlation of case-adjusted concentration (copies/L/case) (left) and PMMoV concentration (right) to daily average flow rate (MGD) in JI (top) and SS (bottom). Outliers in PMMoV analysis were removed for the visual data. P-values including total dataset are included in the text.

The percentage of human fecal contribution had a low, but significant, correlation to flow in both WWTPs (Figure 15) (Kendall's tau, $p < 0.05$), that was stronger in SS (Kendall's tau, $p = 0.008$) than JI (Kendall's tau, $p = 0.035$). Unlike SARS-CoV-2, PMMoV decreased slightly with increasing flows, but not to the extent expected if dilution was occurring.

4.3.3. Influence of BOD and TSS

Overall, there was either no or very low correlation between BOD or TSS and case-adjusted loads. The low negative correlation in JI of BOD to case-adjusted loads was deemed significant (Figure 16), but considering JI had overall higher case-adjusted loads and lower BOD than SS

WWTP (Table 10), we can infer that BOD does not have a substantial effect on SARS-CoV-2 concentration entering the plant.

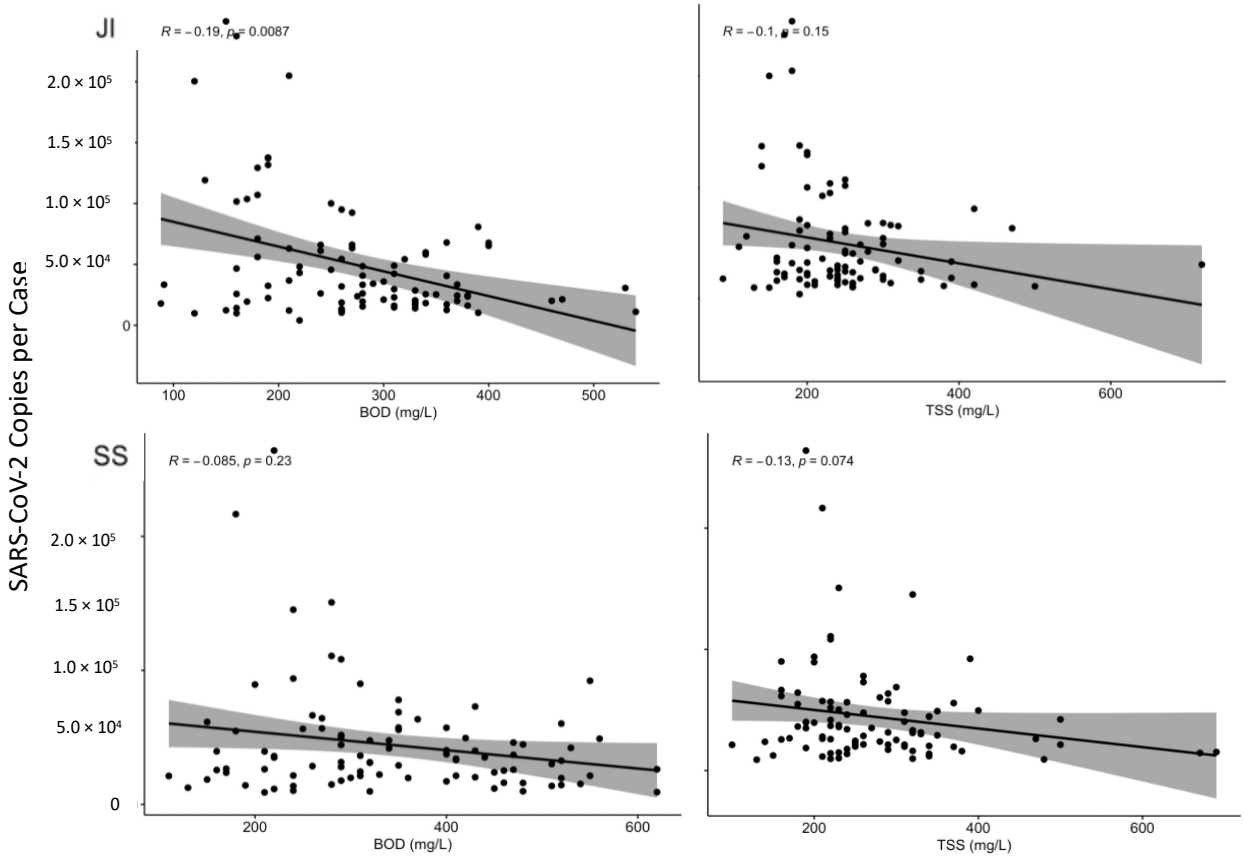

Figure 16. Kendall's rank correlation of BOD (mg/L), and TSS (mg/L) to SARS-CoV-2 copies per case in JI (top) and SS (bottom) WWTPs.

4.*3.4 Influences of Temperature*

SARS-CoV-2 case-adjusted loads were on average 40-55% higher in colder months compared to warmer months in both SS (Welch's t-test, p = 0.04) and JI (Welch's t-test, p = 0.02) suggesting there is less decay in JI and SS conveyance systems in cooler temperatures (Figure 17). These temperature effects occurred, despite the short travel time in the JI service area that would subject SARS-CoV-2 to temperature effects. We further examined that temperature was

significantly negatively correlated to SARS-CoV-2 copies per case in both plants (Kendall's tau, $p < 0.05$). August was the only significant outlier in any grouping for both WWTPs (ANOVA, $p < 0.05$), August also had the highest flow of all warm months (Supplemental Figure 1). For a better sense of the influence of temperature has on concentration, best-fit equations are included in Appendix 3.

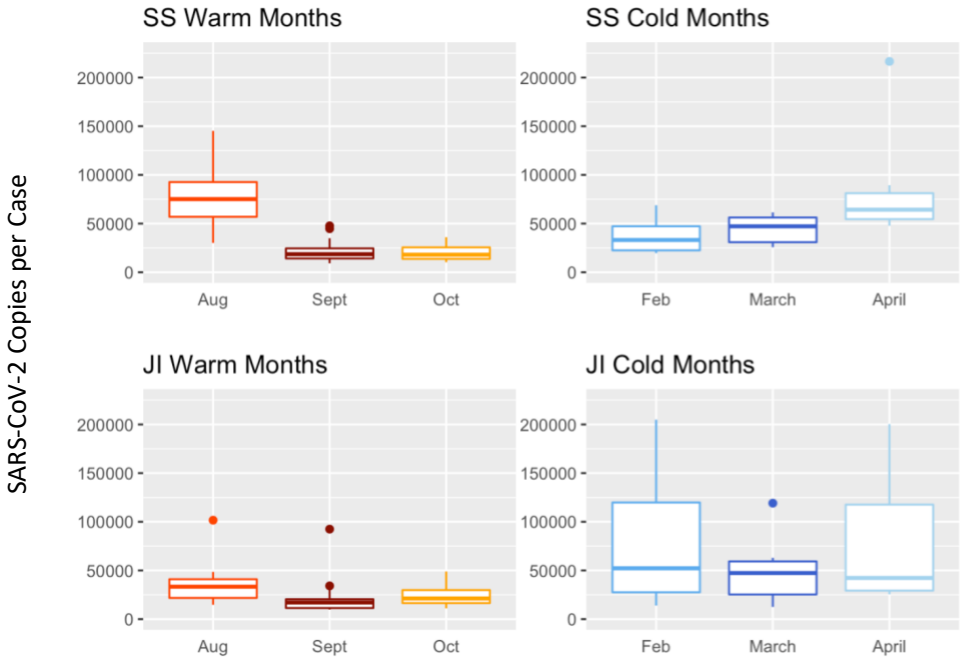

Figure 17. SARS-CoV-2 copies per case during warmest (17.41 – 19.75ºC) and coldest months (8.60 - 12.27ºC) in SS and JI WWTPs.

4.4. Discussion

Wastewater surveillance is increasingly being used by public health officials to monitor COVID-19 prevalence and respond accordingly to help contain and mitigate outbreaks in specific communities [48]. Researchers across the country are implementing this tool, despite critical gaps in the knowledge on how SARS-CoV-2 recovery is affected within untreated

wastewater entering WWTPs [16], [43], [77], [78]. While laboratory-based studies have been performed to determine viral decay under certain temperatures over time [43], [71], our study has the benefit of access to a wastewater system that is highly instrumented for flow and temperature. Both JI and SS fall under the supervision of MMSD which allows the comparison of two treatment plants with different travel times with nearly identical data collection, maintenance, treatment, and supervisory standards. This enabled us to evaluate the impact of various parameters on SARS-CoV-2 concentration within the residence time of a sewer conveyance system. The paired design of the study allowed us to control for common parameters such as temperature or rainfall (increasing flow) when comparing travel times since both systems were subjected to similar environmental conditions.

We hypothesized that under high-flow conditions when travel times are shortest, there would be no difference in copies per case between the two plants. Under low-flow conditions, when travel times are the longest and there is the greatest difference between JI and SS, we would expect to observe difference in SARS-CoV-2 case-adjusted loads. Overall, we found that there was minimal SARS-CoV-2 decay with travel time, suggesting this is not an important parameter to consider in comparisons of different sewer systems.

Wastewater surveillance programs generally use measured concentrations multiplied times flow to calculate the load. Since approximately the same number of people in the service area contribute biological material to the sewer system in high- or low-flow conditions, we expect that SARS-CoV-2 or fecal markers such as PMMoV would be proportionally diluted with the flow. However, we found no effect, where SARS-CoV-2 case-adjusted concentrations were not proportionally reduced. The same analysis with PMMoV also showed no proportional dilution, however, there were slight decreases in PMMoV concentrations in high flow

conditions. Higher flows can result in shorter travel times and less decay which could account for this pattern, but our time travel analysis suggests differences in decay over typical residence times are minimal.

Previous work found calculating loads using flow did not increase the correlation between cases and SARS-CoV-2 concentrations compared with simply using concentrations [46]. High flows result in scouring, which could inject residual SARS-CoV-2 into the waste stream, however, this explanation was also not supported as we did not observe an increased TSS with increased flow. Additional studies are needed to examine how reservoirs might accumulate and be mobilized in conveyance systems, which can span thousands of miles of pipes in urban areas. While most reporting is normalized to flow [54], the practice to include flow in assessing SARS-CoV-2 trends needs further consideration.

We determined that TSS had a negligible effect on SARS-CoV-2 case-adjusted copies detected in wastewater, which is comparable to other literature [79]. And, while BOD was significantly higher in SS than in JI, we can conclude that there was no direct impact of SARS-CoV-2 from BOD because the copies per case were not significantly higher in either plant despite significantly different BOD levels. Further negating significance, JI illustrated a low but significant negative correlation with BOD but had overall lower BOD levels and higher SARS-CoV-2 case-adjusted copies. In addition, BOD is known to be tightly correlated to temperature [80], so this low correlation may be a direct result of temperature.

Temperature had the strongest effect on SARS-CoV-2 viral concentration (Kendall's tau, $p < 0.05$), significantly reducing observed concentration exposed to warmer conditions in JI (paired t-test, $p = 0.02$), and SS (paired t-test, $p = 0.046$). Temperature posing a significant effect

on SARS-CoV-2 decay is consistent with other studies that indicate coronaviruses, and specifically SARS-CoV-2, are sensitive to warmer temperatures [32], [43], [81]–[83] where decay rates for similar temperature windows ranged between 0.021-2.16 k/day [32], [43], [72], [73]. Because increasing temperatures reduce RNA stability, and make it more difficult for any virus to survive [84], the significant results derived from this study's small temperature range is not abnormal. Previous studies have shown that increasing the temperature from just 4°C to 10°C can more than double the decay rate of SARS-CoV-2 RNA, measured through detection of the N1 and N2 gene [83].

In all, temperature is the only parameter crucial to consider when interpreting empirical values for SARS-CoV-2 concentrations in wastewater, especially when combined with longer residence times due to low-flow conditions and extensive sewer networks. The residence time of a sewer conveyance system can change vastly on any given day due to weather conditions, or industrial drainage; it is important to take this into account when determining or applying the decay rate within a sewer network.

Chapter 5. Increasing Sensitivity of SARS-CoV-2 Detection with Primary Settled Solids

5.1 Introduction

The goals of this chapter are to explore how wastewater parameters can be considered to further improve SARS-CoV-2 detection for wastewater surveillance in our laboratory. While Chapter 4 illustrated that influent TSS did not have a significant impact on SARS-CoV-2 detection in wastewater, influent usually only contains around 1 percent total solids. Additionally, studies have shown solids can conglomerate and protect enveloped viruses, such as SARS-CoV-2 [85][86] because the lipid membrane favors binding to solids over liquids [87]. In the wastewater treatment process, raw wastewater enters the primary clarifiers where solids are settled out of the liquid fraction of wastewater (Figure 18) forming a semi-solid slurry referred to as "sludge" that is approximately 3-5 percent solids [88]. Various laboratories use primary settled solids, or sludge, instead of influent for their wastewater surveillance, and have achieved similar detection sensitivity with less sample volume [85]. To further examine if solid content effects SARS-CoV-2 detection levels by protecting RNA, the SARS-CoV-2 concentration extracted from both JI wastewater influent and sludge was compared.

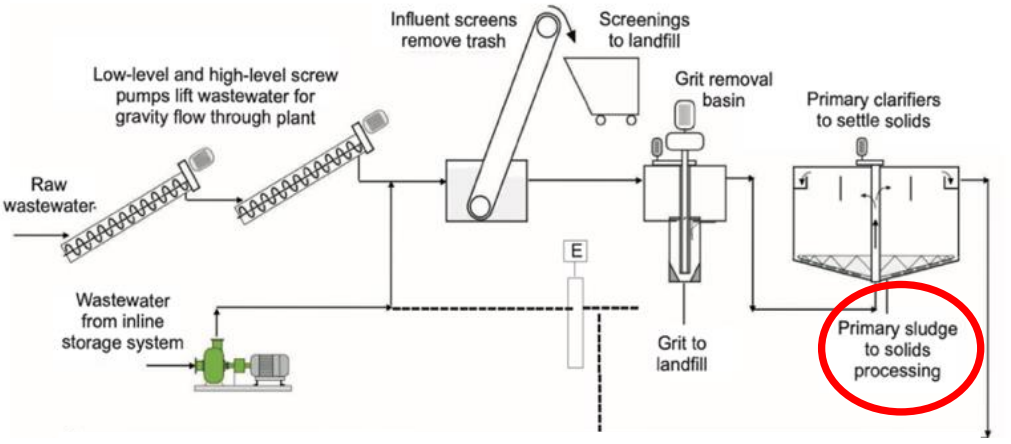

Figure 18. The wastewater treatment process performed at MMSD [18]. The solids used for this analysis are separated from the wastewater liquid phase during primary clarification step (highlighted in red).

5.2 Experimental Specific Methodology

5.2.1 Collection of Sludge Samples

Sludge samples were only collected from JI WWTP due significantly longer hydraulic residence time of the conveyance at SS WWTP. Aliquots were collected by POTW staff once every 4 hours and composited over a 24-hour period using sterile 50 mL falcon tubes. In total, 6 grab samples were performed for each sample composite. Composites are stored 4°C, until in-person pick-up, and delivery on-ice. Once received in the lab, samples are stored at 4°C until they were processed within 24 hours. In total, 25 sludge samples collected weekly from August 25, 2021, to February 23, 2022, were used in this analysis.

5.2.2 Processing Sludge Samples

40 mL of sludge solids were dewatered by centrifugation at 124,000 g-force for 30 minutes at 4°C, and the supernatant is disposed of in bleach. Approximately 0.075 grams dewatered solids are removed as required for nucleic acid extraction, and the remaining solids are used to calculate the dry weight of the dewatered solids. The dry weight of the sample was recorded by measuring the weight of each dewatered-solids sample before and after heating at 75°C for at least 24 hours.

5.2.3 RNA Extraction of Sludge Samples

Approximately 0.075 g dewatered solids were suspended in DNA/RNA shield (Zymo Research, CA) spiked with approximately 100,000 copies (1.5 μL) BCoV (Calf-guard Cattle Vaccine, PBS Animal Health, OH). Resuspended samples were stored at -80°C (up to 24 hours)

to increase RNA extraction yield until the nucleic acid extraction. Samples were allowed to completely thaw on ice before bead beating for 2.5 minutes, resting on ice, and repeating before loading into the King Fisher instrument, following the same extraction procedures as the JI influent described in Chapter 2.2.4.

5.2.5 Data Analysis

This analysis compared all 25 sludge samples to 25 influent samples paired by date from JI. SARS-CoV-2 concentration per capita (copies per person) in suspended solids (C_{solids}) can be approximated using Equation 6. Where C_{dry} is the copies per gram of solids per dry weight of our 24-hour composite sample, *Q* is average daily flow in liters (L) of influent, *T* is the daily average total solids of the sludge in grams per liter (g/L), and *P* is the population of JI sewershed (470,000 people).

$$C_{solids} = \frac{C_{dry} * Q}{T * P} \quad (6)$$

SARS-CoV-2 per of both sludge and influent were compared. Because the unit for sludge concentration per capita is in copies per gram of solids, and the unit for influent is in copies per liter of wastewater, RT-ddPCR droplet data was also compared since there is no true conversion between liters and grams. Paired- t-tests were performed to determine if the primary settles solids in sludge have a significant impact on SARS-CoV-2 concentration when comparing to wastewater influent, and nonparametric Kendall's tau was used to test if either method had a better correlation between the clinical case rate confirmed in the JI sewershed and the SARS-CoV-2 concentration detected from the sample.

5.3 Results and Discussion

SARS-CoV-2 concentrations per capita in matched sludge and influent samples were positively and significantly correlated (Kendall's tau, $p < 0.005$). When comparing both the detected RT-ddPCR positive droplets, and the SARS-CoV-2 concentration per capita, sludge samples were significantly higher than in the influent samples from the same date (Paired t-test, $p < 0.005$). Quantifying SARS-CoV-2 concentration from sludge produces up to two orders of magnitude higher average concentration (Figure 19) than wastewater influent, indicating that recovery may be better when comparing the solid versus liquid portion of wastewater.

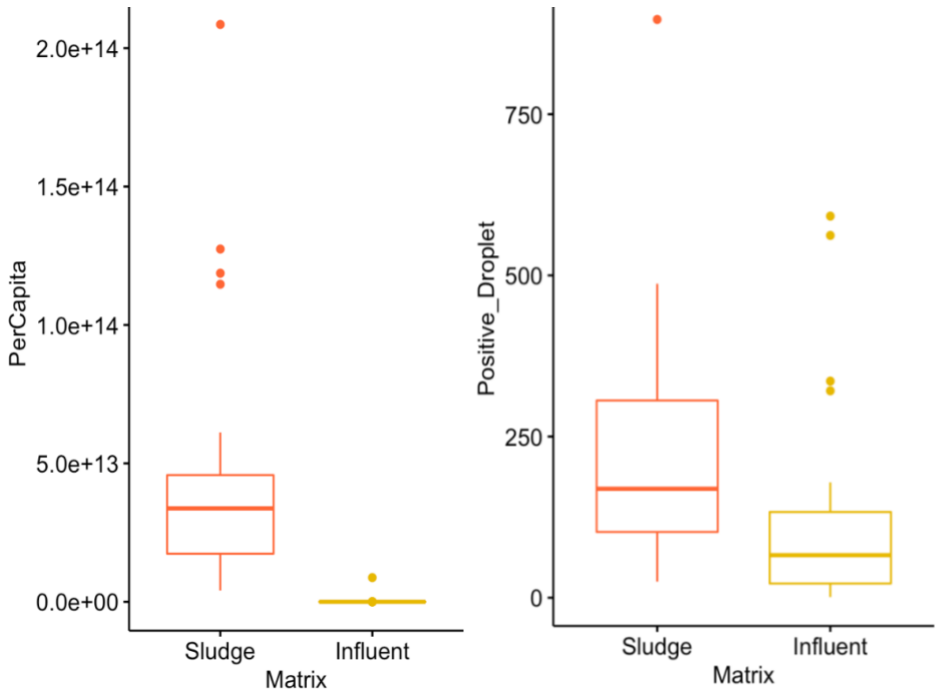

Measurement	Sludge	Influent
Mean	4.69E+13	3.49E+11
SD	4.76E+13	1.75E+12
Median	3.37E+13	3.20E+11
IQR	2.84E+13	6.87E+11

Measurement	Sludge	Influent
Mean	220	126
SD	185	162
Median	169	66
IQR	204	111

Figure 19. Box plot of the total per capita SARS-CoV-2 concentration (left) and N1/N2 droplets detected by RT-ddPCR (right) in the sludge (orange) and influent (yellow) data sets (n = 25).

This conclusion agrees with previously published literature that have concluded both SARS-CoV-2 and PMMoV RNA are enriched in the solid fraction of wastewater [85][89][90]. While this was a relatively small dataset, two influent samples were below LOQ, with one falling below LOD. No sludge samples were below the LOQ. In addition, the droplet detection of N1 and N2 in sludge is on average double that of its influent counterpart (Figure 19). This data suggests that quantification of RNA from sludge is more sensitive when concentrations are low, and extraction of SARS-CoV-2 RNA from sludge can be used when community levels are so low that they may go undetected.

Both sludge and influent SARS-CoV-2 concentration per capita were positively and significantly correlated to the detected clinical cases within the JI sewershed (Kendall's tau, $p < 0.005$), with influent having a slightly better linear relationship (Figure 20).

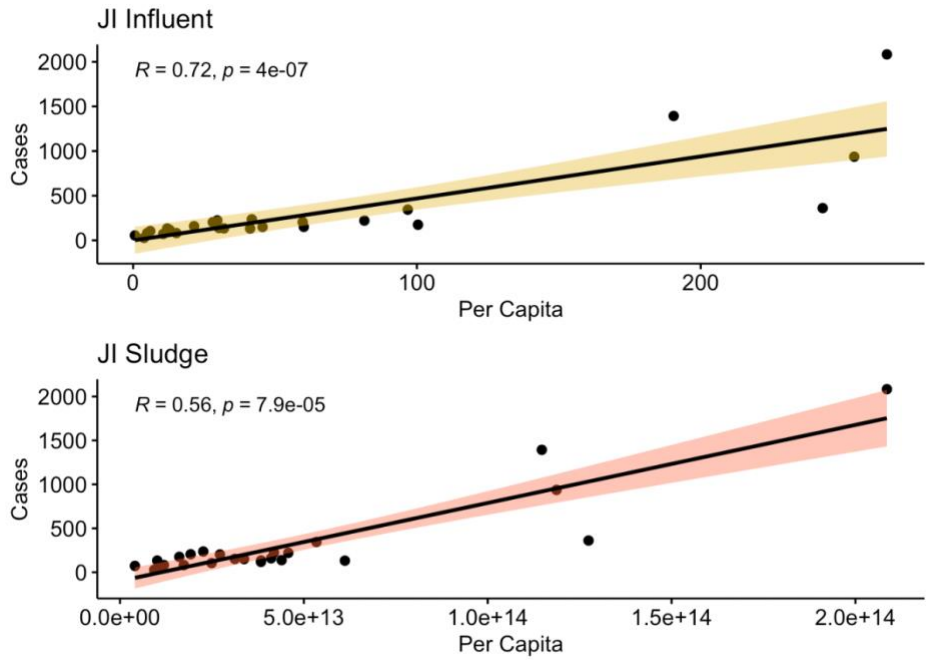

Figure 20. Kendall's tau correlation of SARS-CoV-2 concentration per capita to number of clinical cases within the JI sewershed extracted from influent (yellow) and sludge (orange) samples.

While it is important to confirm sludge and influent are reliable methods for monitoring COVID-19, as mentioned in Chapter 4, COVID-19 case rate data is not completely reliable for monitoring prevalence due to under-reporting and other clinical testing data biases [57]. It is more important for wastewater surveillance to capture COVID-19 infection trends, such as rapid increases. Shifts in trends were adequately represented in sludge (Figure 21).

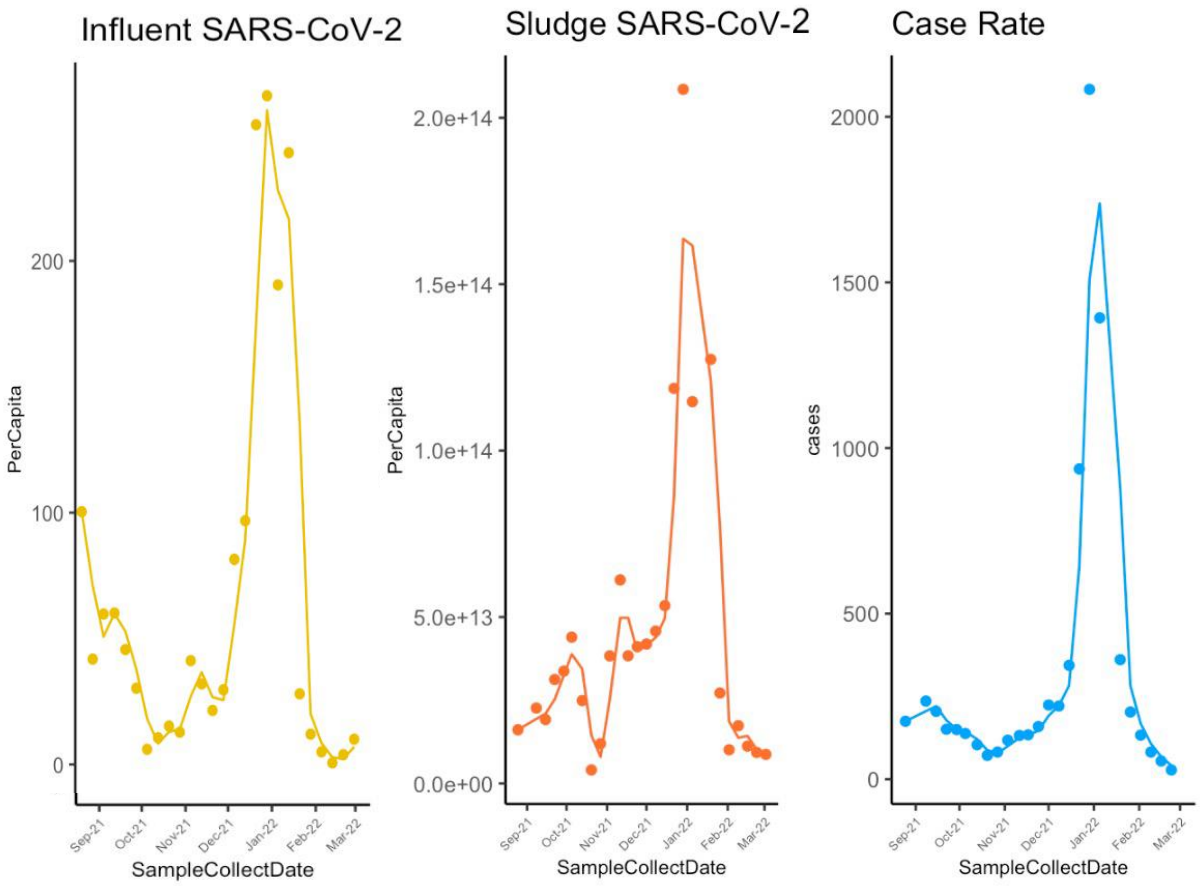

Figure 21. SARS-CoV-2 concentration per capita, and two-day moving average extracted from influent (yellow) and sludge (orange) samples plotted by the clinical case rate of the JI sewershed (blue).

Chapter 6. Conclusions and Future Work

This project investigated various factors that may diminish or improve the capability of wastewater surveillance as a public health aid for the COVID-19 epidemic. The results showed that laboratory methods can be used to increase the sensitivity of SARS-CoV-2 detection, such as automated magnetic-bead-based RNA extraction. That monitoring COVID-19 variants through RT-ddPCR analysis can be more representative than traditional public health metrics such as clinical sequencing. While there are numerous wastewater parameters that can impact SARS-CoV-2 persistence and detection, warm temperatures were the only parameter in this study found to have a measurable impact within the residence time of an average sewer network. And, that analyzing primary solids within wastewater instead of influent may double the sensitivity of SARS-CoV-2 detection. Overall, this study further confirms what laboratories across the world have already hypothesized and demonstrated; that wastewater surveillance is a reliable metric for monitoring COVID-19 infection trends within a specific community [15][17][45][70][86][89][90][91].

As we see COVID-19 declining and evolving, we can use the study of SARS-CoV-2 wastewater surveillance to help standardize laboratory techniques, and better understand how it can be used for future applications, such as under-reported, new, or evolving viruses. When compared to other public health tools, wastewater surveillance noninvasively and comprehensively tracks infectious disease spread and resistance throughout a community in a cost- and supply-effective manner. Wastewater surveillance was able to detect mutations and emerging variants prior to clinical sequencing data in various communities across Wisconsin. Outside of infectious disease prevalence, wastewater surveillance could use used to track a wide

array of things such as drug and pharmaceutical use, antimicrobial resistance, and chemical exposure [91]. Validation of using wastewater surveillance to track COVID-19 would be a step in the right direction for other implications of wastewater surveillance to take off. Based the positive results our lab has observed from SARS-CoV-2 wastewater surveillance, we have already began working with Wisconsin DHS to monitor Influenza A and Influenza B, and antimicrobial resistance in Wisconsin. The results of this study should prove useful in the expansion of labs our wastewater surveillance projects, in addition to other research laboratories, municipalities, public health officials, and policy makers who are seeking to monitor specific viral, biological, or chemical targets in a noninvasive, comprehensive, and cost-effective manner.

REFRENCES

[1] Committee on Economic, Social, and Cultural Rights (CESCR), “Economic and Social Council: SUBSTANTIVE ISSUES ARISING IN THE IMPLEMENTATION OF THE INTERNATIONAL COVENANT ON ECONOMIC, SOCIAL AND CULTURAL RIGHTS.” 2000. [Online]. Available: https://digitallibrary.un.org/record/442869?ln=en

[2] World Health Organization (WHO), “Human rights and health.,” 2017. [Online]. Available: https://www.who.int/news-room/fact-sheets/detail/human-rights-and-health

[3] World Health Organization (WHO), “Preventing epidemics and pandemics.,” 2021. [Online]. Available: https://www.who.int/activities/preventing-epidemics-and-pandemics

[4] Assistant Secretary for Public Affairs (ASPA), “About HHS. U.S. Department of Health & Human Services.,” 2021. [Online]. Available: https://www.hhs.gov/about/index.html

[5] Centers for Disease Control and Prevention (CDC), “Mission, Role and Pledge. U.S. Department of Health and Human Services.,” 2019. [Online]. Available: https://www.cdc.gov/about/organization/mission.htm

[6] Coronaviridae Study Group of the International Committee on Taxonomy of Viruses, “The species Severe acute respiratory syndrome-related coronavirus: classifying 2019-nCoV and naming it SARS-CoV-2,” *Nat Microbiol*, vol. 5, no. 4, pp. 536–544, Apr. 2020, doi: 10.1038/s41564-020-0695-z.

[7] H. Ritchie *et al.*, “Coronavirus Pandemic (COVID-19),” 2020, [Online]. Available: 'https://ourworldindata.org/coronavirus'

[8] Worldometers.info, “COVID-19 CORONAVIRUS PANDEMIC,” 2022, [Online]. Available: https://www.worldometers.info/coronavirus/#countries

[9] Q. Li *et al.*, “Early Transmission Dynamics in Wuhan, China, of Novel Coronavirus–Infected Pneumonia,” *N Engl J Med*, vol. 382, no. 13, pp. 1199–1207, Mar. 2020, doi: 10.1056/NEJMoa2001316.

[10] D. Cennimo, S. Bergman, and K. Olsen, “Coronavirus Disease 2019 (COVID-19),” *MedScape*, 2022.

[11] S. A. Lauer *et al.*, “The Incubation Period of Coronavirus Disease 2019 (COVID-19) From Publicly Reported Confirmed Cases: Estimation and Application,” *Annals of Internal Medicine*, vol. 172, no. 9, pp. 577–582, May 2020, doi: 10.7326/M20-0504.

[12] Centers for Disease Control and Prevention (CDC), “Symptoms of Coronavirus. U.S. Department of Health and Human Services.,” 2020. [Online]. Available: https://www.cdc.gov/coronavirus/2019-ncov/symptoms-testing/symptoms.html

[13] R. Li *et al.*, “Substantial undocumented infection facilitates the rapid dissemination of novel coronavirus (SARS-CoV-2),” *Science*, vol. 368, no. 6490, pp. 489–493, May 2020, doi: 10.1126/science.abb3221.

[14] K. G. Andersen, A. Rambaut, W. I. Lipkin, E. C. Holmes, and R. F. Garry, “The proximal origin of SARS-CoV-2,” *Nat Med*, vol. 26, no. 4, pp. 450–452, Apr. 2020, doi: 10.1038/s41591-020-0820-9.

[15] N. Sims and B. Kasprzyk-Hordern, “Future perspectives of wastewater-based epidemiology: Monitoring infectious disease spread and resistance to the community level,” *Environment International*, vol. 139, p. 105689, Jun. 2020, doi: 10.1016/j.envint.2020.105689.

[16] G. La Rosa *et al.*, "Surveillance of hepatitis A virus in urban sewages and comparison with cases notified in the course of an outbreak, Italy 2013," *BMC Infect Dis*, vol. 14, no. 1, p. 419, Dec. 2014, doi: 10.1186/1471-2334-14-419.
[17] A. E. Kirby *et al.*, "Using Wastewater Surveillance Data to Support the COVID-19 Response — United States, 2020–2021," *MMWR Morb. Mortal. Wkly. Rep.*, vol. 70, no. 36, pp. 1242–1244, Sep. 2021, doi: 10.15585/mmwr.mm7036a2.
[18] R. J. Newton *et al.*, "Sewage Reflects the Microbiomes of Human Populations," *mBio*, vol. 6, no. 2, pp. e02574-14, May 2015, doi: 10.1128/mBio.02574-14.
[19] MMSD, "Treatment Process," 2022, [Online]. Available: https://www.mmsd.com/what-we-do/wastewater-treatment/treatment-process
[20] M. C. Almeida, D. Butler, and E. Friedler, "At-source domestic wastewater quality," *Urban Water*, vol. 1, no. 1, pp. 49–55, Mar. 1999, doi: 10.1016/S1462-0758(99)00008-4.
[21] C. P. Gerba, W. Q. Betancourt, and M. Kitajima, "How much reduction of virus is needed for recycled water: A continuous changing need for assessment?," *Water Research*, vol. 108, pp. 25–31, Jan. 2017, doi: 10.1016/j.watres.2016.11.020.
[22] K. Rosario, E. M. Symonds, C. Sinigalliano, J. Stewart, and M. Breitbart, "Pepper mild mottle virus as an indicator of fecal pollution," *Appl Environ Microbiol*, vol. 75, no. 22, pp. 7261–7267, Nov. 2009, doi: 10.1128/AEM.00410-09.
[23] CDC, "Wastewater Surveillance Testing Methods," 2020, [Online]. Available: https://www.cdc.gov/healthywater/surveillance/wastewater-surveillance/testing-methods.htmlms
[24] B. M. Pecson *et al.*, "Reproducibility and sensitivity of 36 methods to quantify the SARS-CoV-2 genetic signal in raw wastewater: findings from an interlaboratory methods evaluation in the U.S.," *Environ. Sci.: Water Res. Technol.*, vol. 7, no. 3, pp. 504–520, 2021, doi: 10.1039/D0EW00946F.
[25] Z. W. LaTurner *et al.*, "Evaluating recovery, cost, and throughput of different concentration methods for SARS-CoV-2 wastewater-based epidemiology," *Water Research*, vol. 197, p. 117043, Jun. 2021, doi: 10.1016/j.watres.2021.117043.
[26] Y. Chen *et al.*, "The presence of SARS-CoV-2 RNA in the feces of COVID-19 patients," *J Med Virol*, vol. 92, no. 7, pp. 833–840, Jul. 2020, doi: 10.1002/jmv.25825.
[27] T. Boogaerts *et al.*, "Current and future perspectives for wastewater-based epidemiology as a monitoring tool for pharmaceutical use," *Science of The Total Environment*, vol. 789, p. 148047, Oct. 2021, doi: 10.1016/j.scitotenv.2021.148047.
[28] CDC, "2019-Novel Coronavirus (2019-nCoV) Real-time rRT-PCR Panel Primers and Probe," *Division of Viral Diseases, National Center for Immunization and Respiratory Diseases, Centers for Disease Control and Prevention*, May 2020.
[29] N. Decaro *et al.*, "Detection of bovine coronavirus using a TaqMan-based real-time RT-PCR assay," *Journal of Virological Methods*, vol. 151, no. 2, pp. 167–171, Aug. 2008, doi: 10.1016/j.jviromet.2008.05.016.
[30] M. Kishimoto *et al.*, "Development of a one-run real-time PCR detection system for pathogens associated with bovine respiratory disease complex," *The Journal of Veterinary Medical Science*, vol. 79, no. 3, pp. 517–523, 2017, doi: 10.1292/jvms.16-0489.
[31] T. Zhang *et al.*, "RNA Viral Community in Human Feces: Prevalence of Plant Pathogenic Viruses," *PLoS Biol*, vol. 4, no. 1, p. e3, Dec. 2005, doi: 10.1371/journal.pbio.0040003.

[32] J. Weidhaas *et al.*, "Correlation of SARS-CoV-2 RNA in wastewater with COVID-19 disease burden in sewersheds," *Science of The Total Environment*, vol. 775, p. 145790, Jun. 2021, doi: 10.1016/j.scitotenv.2021.145790.
[33] I. L. Lo *et al.*, "Evaluation of SARS-CoV-2 RNA shedding in clinical specimens and clinical characteristics of 10 patients with COVID-19 in Macau," *Int. J. Biol. Sci.*, vol. 16, no. 10, pp. 1698–1707, 2020, doi: 10.7150/ijbs.45357.
[34] Y. Zhang *et al.*, "Prevalence and Persistent Shedding of Fecal SARS-CoV-2 RNA in Patients With COVID-19 Infection: A Systematic Review and Meta-analysis," *Clin Transl Gastroenterol*, vol. 12, no. 4, p. e00343, Apr. 2021, doi: 10.14309/ctg.0000000000000343.
[35] L. Zou *et al.*, "SARS-CoV-2 Viral Load in Upper Respiratory Specimens of Infected Patients," *N Engl J Med*, vol. 382, no. 12, pp. 1177–1179, Mar. 2020, doi: 10.1056/NEJMc2001737.
[36] S. Parasa *et al.*, "Prevalence of Gastrointestinal Symptoms and Fecal Viral Shedding in Patients With Coronavirus Disease 2019: A Systematic Review and Meta-analysis," *JAMA Netw Open*, vol. 3, no. 6, p. e2011335, Jun. 2020, doi: 10.1001/jamanetworkopen.2020.11335.
[37] Y. Wu *et al.*, "Prolonged presence of SARS-CoV-2 viral RNA in faecal samples," *The Lancet Gastroenterology & Hepatology*, vol. 5, no. 5, pp. 434–435, May 2020, doi: 10.1016/S2468-1253(20)30083-2.
[38] S. Zheng *et al.*, "Viral load dynamics and disease severity in patients infected with SARS-CoV-2 in Zhejiang province, China, January-March 2020: retrospective cohort study," *BMJ*, p. m1443, Apr. 2020, doi: 10.1136/bmj.m1443.
[39] Y. Xu *et al.*, "Characteristics of pediatric SARS-CoV-2 infection and potential evidence for persistent fecal viral shedding," *Nat Med*, vol. 26, no. 4, pp. 502–505, Apr. 2020, doi: 10.1038/s41591-020-0817-4.
[40] M. A. De Ioris *et al.*, "Dynamic Viral Severe Acute Respiratory Syndrome Coronavirus 2 RNA Shedding in Children: Preliminary Data and Clinical Consideration from a Italian Regional Center," *Journal of the Pediatric Infectious Diseases Society*, vol. 9, no. 3, pp. 366–369, Jul. 2020, doi: 10.1093/jpids/piaa065.
[41] Y. Ling *et al.*, "Persistence and clearance of viral RNA in 2019 novel coronavirus disease rehabilitation patients," *Chinese Medical Journal*, vol. 133, no. 9, pp. 1039–1043, May 2020, doi: 10.1097/CM9.0000000000000774.
[42] T. W. R. F. (WRF), "Wastewater Surveillance of the COVID-19 Genetic Signal in Sewersheds: Recommendations from Global Experts," 2020.
[43] W. Ahmed *et al.*, "Decay of SARS-CoV-2 and surrogate murine hepatitis virus RNA in untreated wastewater to inform application in wastewater-based epidemiology," *Environmental Research*, vol. 191, p. 110092, Dec. 2020, doi: 10.1016/j.envres.2020.110092.
[44] S. Yang *et al.*, "Persistence of SARS-CoV-2 RNA in wastewater after the end of the COVID-19 epidemics," *Journal of Hazardous Materials*, vol. 429, p. 128358, May 2022, doi: 10.1016/j.jhazmat.2022.128358.
[45] M. Achak, S. Alaoui Bakri, Y. Chhiti, F. E. M'hamdi Alaoui, N. Barka, and W. Boumya, "SARS-CoV-2 in hospital wastewater during outbreak of COVID-19: A review on detection, survival and disinfection technologies," *Science of The Total Environment*, vol. 761, p. 143192, Mar. 2021, doi: 10.1016/j.scitotenv.2020.143192.

[46] S. Feng *et al.*, "Evaluation of Sampling, Analysis, and Normalization Methods for SARS-CoV-2 Concentrations in Wastewater to Assess COVID-19 Burdens in Wisconsin Communities," *ACS EST Water*, vol. 1, no. 8, pp. 1955–1965, Aug. 2021, doi: 10.1021/acsestwater.1c00160.
[47] C. Wallis, M. Henderson, and J. L. Melnick, "Enterovirus Concentration on Cellulose Membranes," *Appl Microbiol*, vol. 23, no. 3, pp. 476–480, Mar. 1972, doi: 10.1128/am.23.3.476-480.1972.
[48] A. E. Kirby *et al.*, "Using Wastewater Surveillance Data to Support the COVID-19 Response — United States, 2020–2021," *MMWR Morb. Mortal. Wkly. Rep.*, vol. 70, no. 36, pp. 1242–1244, Sep. 2021, doi: 10.15585/mmwr.mm7036a2.
[49] E. J. Palmer *et al.*, "Development of a reproducible method for monitoring SARS-CoV-2 in wastewater," *Science of The Total Environment*, vol. 799, p. 149405, Dec. 2021, doi: 10.1016/j.scitotenv.2021.149405.
[50] C. Ambrosi *et al.*, "SARS-CoV-2: Comparative analysis of different RNA extraction methods," *Journal of Virological Methods*, vol. 287, p. 114008, Jan. 2021, doi: 10.1016/j.jviromet.2020.114008.
[51] WI DHS, "COVID-19: Wisconsin Coronavirus Wastewater Monitoring Network," 2020, [Online]. Available: https://www.dhs.wisconsin.gov/covid-19/wastewater.htm
[52] D. A. Armbruster and T. Pry, "Limit of blank, limit of detection and limit of quantitation," *Clin Biochem Rev*, vol. 29 Suppl 1, pp. S49-52, Aug. 2008.
[53] H. D. Greenwald *et al.*, "Tools for interpretation of wastewater SARS-CoV-2 temporal and spatial trends demonstrated with data collected in the San Francisco Bay Area," *Water Research X*, vol. 12, p. 100111, Aug. 2021, doi: 10.1016/j.wroa.2021.100111.
[54] G. Medema, L. Heijnen, G. Elsinga, R. Italiaander, and A. Brouwer, "Presence of SARS-Coronavirus-2 RNA in Sewage and Correlation with Reported COVID-19 Prevalence in the Early Stage of the Epidemic in The Netherlands," *Environ. Sci. Technol. Lett.*, vol. 7, no. 7, pp. 511–516, Jul. 2020, doi: 10.1021/acs.estlett.0c00357.
[55] R Core Team, "R: A language and environment for statistical computing. R Foundation for Statistical Computing, Vienna, Austria.," *R Foundation for Statistical Computing*, 2020, [Online]. Available: http://www.r-project.org/index.html
[56] M. K. Schussman, A. Roguet, A. Schmoldt, B. Dinan, and S. L. McLellan, "Wastewater surveillance using ddPCR reveals highly accurate tracking of Omicron variant due to altered N1 probe binding efficiency," Public and Global Health, preprint, Feb. 2022. doi: 10.1101/2022.02.18.22271188.
[57] L. Wang and G. Cheng, "Sequence analysis of the emerging SARS-CoV-2 variant Omicron in South Africa," *Journal of Medical Virology*, vol. 94, no. 4, pp. 1728–1733, Apr. 2022, doi: 10.1002/jmv.27516.
[58] New England Biolabs, "Variants Observed by Genomic Locus and Geographic Region," *GISAID*, 2021.
[59] Y. Bei, K. B. Vrtis, J. G. Borgaro, B. W. Langhorst, and N. M. Nichols, "The Omicron variant mutation at position 28,311 in the SARS-CoV-2 N gene does not perturb CDC N1 target detection," Genetic and Genomic Medicine, preprint, Dec. 2021. doi: 10.1101/2021.12.16.21267734.
[60] Applied Biosystems, "TaqMan SARS-CoV-2 Mutation Panel," *Thermo Fisher Scientific*.

[61] S. Smith, “The effects of sequence length and oligonucleotide mismatches on 5’ exonuclease assay efficiency,” *Nucleic Acids Research*, vol. 30, no. 20, pp. 111e–1111, Oct. 2002, doi: 10.1093/nar/gnf110.
[62] K. A. Khan and P. Cheung, “Presence of mismatches between diagnostic PCR assays and coronavirus SARS-CoV-2 genome,” *R. Soc. open sci.*, vol. 7, no. 6, p. 200636, Jun. 2020, doi: 10.1098/rsos.200636.
[63] B. Süß, G. Flekna, M. Wagner, and I. Hein, “Studying the effect of single mismatches in primer and probe binding regions on amplification curves and quantification in real-time PCR,” *Journal of Microbiological Methods*, vol. 76, no. 3, pp. 316–319, Mar. 2009, doi: 10.1016/j.mimet.2008.12.003.
[64] GISAID, “GISAID EpiCoV™ Database,” *Freunde von GISAID e.V.*, 2022.
[65] A. E. Kirby *et al.*, “Notes from the Field: Early Evidence of the SARS-CoV-2 B.1.1.529 (Omicron) Variant in Community Wastewater — United States, November–December 2021,” *MMWR Morb. Mortal. Wkly. Rep.*, vol. 71, no. 3, pp. 103–105, Jan. 2022, doi: 10.15585/mmwr.mm7103a5.
[66] L. Vallejo, M. Martínez-Rodríguez, M. J. Nieto-Bazán, A. Delgado-Iribarren, and E. Culebras, “Comparative study of different SARS-CoV-2 diagnostic techniques,” *Journal of Virological Methods*, vol. 298, p. 114281, Dec. 2021, doi: 10.1016/j.jviromet.2021.114281.
[67] A. D. Iuliano *et al.*, “Trends in Disease Severity and Health Care Utilization During the Early Omicron Variant Period Compared with Previous SARS-CoV-2 High Transmission Periods - United States, December 2020-January 2022,” *MMWR Morb Mortal Wkly Rep*, vol. 71, no. 4, pp. 146–152, Jan. 2022, doi: 10.15585/mmwr.mm7104e4.
[68] M. K. Schussman and S. L. McLellan, “Effect of Time and Temperature on SARS-CoV-2 in Municipal Wastewater Conveyance Systems,” *Water*, vol. 14, no. 9, p. 1373, Apr. 2022, doi: 10.3390/w14091373.
[69] K. A. Adedokun, A. O. Olarinmoye, J. O. Mustapha, and R. T. Kamorudeen, “A close look at the biology of SARS-CoV-2, and the potential influence of weather conditions and seasons on COVID-19 case spread,” *Infect Dis Poverty*, vol. 9, no. 1, p. 77, Dec. 2020, doi: 10.1186/s40249-020-00688-1.
[70] D. Polo *et al.*, “Making waves: Wastewater-based epidemiology for COVID-19 – approaches and challenges for surveillance and prediction,” *Water Research*, vol. 186, p. 116404, Nov. 2020, doi: 10.1016/j.watres.2020.116404.
[71] P. M. Gundy, C. P. Gerba, and I. L. Pepper, “Survival of Coronaviruses in Water and Wastewater,” *Food Environ Virol*, vol. 1, no. 1, p. 10, Mar. 2009, doi: 10.1007/s12560-008-9001-6.
[72] A.-M. Hokajärvi *et al.*, “The detection and stability of the SARS-CoV-2 RNA biomarkers in wastewater influent in Helsinki, Finland,” *Science of The Total Environment*, vol. 770, p. 145274, May 2021, doi: 10.1016/j.scitotenv.2021.145274.
[73] L. Roldan-Hernandez, K. E. Graham, D. Duong, and A. B. Boehm, “Persistence of endogenous SARS-CoV-2 and pepper mild mottle virus RNA in wastewater settled solids,” Infectious Diseases (except HIV/AIDS), preprint, Jan. 2022. doi: 10.1101/2022.01.06.22268855.
[74] Y. Ye, R. M. Ellenberg, K. E. Graham, and K. R. Wigginton, “Survivability, Partitioning, and Recovery of Enveloped Viruses in Untreated Municipal Wastewater,” *Environ. Sci. Technol.*, vol. 50, no. 10, pp. 5077–5085, May 2016, doi: 10.1021/acs.est.6b00876.

[75] A. H. S. Chik *et al.*, "Comparison of approaches to quantify SARS-CoV-2 in wastewater using RT-qPCR: Results and implications from a collaborative inter-laboratory study in Canada," *Journal of Environmental Sciences*, vol. 107, pp. 218–229, Sep. 2021, doi: 10.1016/j.jes.2021.01.029.
[76] R. S. Kantor, K. L. Nelson, H. D. Greenwald, and L. C. Kennedy, "Challenges in Measuring the Recovery of SARS-CoV-2 from Wastewater," *Environ. Sci. Technol.*, vol. 55, no. 6, pp. 3514–3519, Mar. 2021, doi: 10.1021/acs.est.0c08210.
[77] M. Kitajima *et al.*, "SARS-CoV-2 in wastewater: State of the knowledge and research needs," *Science of The Total Environment*, vol. 739, p. 139076, Oct. 2020, doi: 10.1016/j.scitotenv.2020.139076.
[78] A. I. Silverman and A. B. Boehm, "Systematic Review and Meta-Analysis of the Persistence and Disinfection of Human Coronaviruses and Their Viral Surrogates in Water and Wastewater," *Environ. Sci. Technol. Lett.*, vol. 7, no. 8, pp. 544–553, Aug. 2020, doi: 10.1021/acs.estlett.0c00313.
[79] J. Carrillo-Reyes, M. Barragán-Trinidad, and G. Buitrón, "Surveillance of SARS-CoV-2 in sewage and wastewater treatment plants in Mexico," *Journal of Water Process Engineering*, vol. 40, p. 101815, Apr. 2021, doi: 10.1016/j.jwpe.2020.101815.
[80] T. M. Flegal and E. D. Schroeder, "Temperature Effects on BOD Stoichiometry and Oxygen Uptake Rate," *Water Pollution Control Federation*, vol. 48, no. 12, Dec. 1976, [Online]. Available: https://www.jstor.org/stable/25040084
[81] M. K. Ijaz, S. A. Sattar, C. M. Johnson-Lussenburg, and V. S. Springthorpe, "Comparison of the airborne survival of calf rotavirus and poliovirus type 1 (Sabin) aerosolized as a mixture," *Appl Environ Microbiol*, 1985.
[82] A. Bivins *et al.*, "Persistence of SARS-CoV-2 in Water and Wastewater," *Environ. Sci. Technol. Lett.*, vol. 7, no. 12, pp. 937–942, Dec. 2020, doi: 10.1021/acs.estlett.0c00730.
[83] L. C. de Oliveira *et al.*, "Viability of SARS-CoV-2 in river water and wastewater at different temperatures and solids content," *Water Research*, vol. 195, p. 117002, May 2021, doi: 10.1016/j.watres.2021.117002.
[84] Y. Chi, Q. Wang, G. Chen, and S. Zheng, "The Long-Term Presence of SARS-CoV-2 on Cold-Chain Food Packaging Surfaces Indicates a New COVID-19 Winter Outbreak: A Mini Review," *Front. Public Health*, vol. 9, p. 650493, May 2021, doi: 10.3389/fpubh.2021.650493.
[85] S. Kim *et al.*, "SARS-CoV-2 RNA is enriched by orders of magnitude in primary settled solids relative to liquid wastewater at publicly owned treatment works," *Environ. Sci.: Water Res. Technol.*, p. 10.1039.D1EW00826A, 2022, doi: 10.1039/D1EW00826A.
[86] B. Li, D. Y. W. Di, P. Saingam, M. K. Jeon, and T. Yan, "Fine-Scale Temporal Dynamics of SARS-CoV-2 RNA Abundance in Wastewater during A COVID-19 Lockdown," *Water Research*, vol. 197, p. 117093, Jun. 2021, doi: 10.1016/j.watres.2021.117093.
[87] C. J. van Oss, *Interfacial Forces in Aqueous Media*, 0 ed. CRC Press, 2006. doi: 10.1201/9781420015768.
[88] "Jones Island O&M Manual." MMSD, Jun. 2020.
[89] P. M. D'Aoust *et al.*, "Quantitative analysis of SARS-CoV-2 RNA from wastewater solids in communities with low COVID-19 incidence and prevalence," *Water Research*, vol. 188, p. 116560, Jan. 2021, doi: 10.1016/j.watres.2020.116560.

[90] K. E. Graham *et al.*, “SARS-CoV-2 RNA in Wastewater Settled Solids Is Associated with COVID-19 Cases in a Large Urban Sewershed,” *Environ. Sci. Technol.*, vol. 55, no. 1, pp. 488–498, Jan. 2021, doi: 10.1021/acs.est.0c06191.
[91] J. O’Keeffe, “Wastewater-based epidemiology: current uses and future opportunities as a public health surveillance tool,” *Environ. Health Rev.*, vol. 64, no. 3, pp. 44–52, Nov. 2021, doi: 10.5864/d2021-015.
[92] A. B. Boehm, A. I. Silverman, A. Schriewer, and K. Goodwin, “Systematic review and meta-analysis of decay rates of waterborne mammalian viruses and coliphages in surface waters,” *Water Research*, vol. 164, p. 114898, Nov. 2019, doi: 10.1016/j.watres.2019.114898.

APPENDICIES

Appendix 1. Supplemental Tables and Figures for Chapter 4

Supplemental Table 1: Estimated travel times accounting for pipe diversions.

Plant	Wet Conditions*	Wet no Diversion	Ave Conditions	Dry Conditions
JI	5.25	4.68	7.45	11.36
SS	13.17	12.88	22.16	63.45

*Pipe diversions account for a 50% decrease in JI acreage and 10% increase in SS acreage

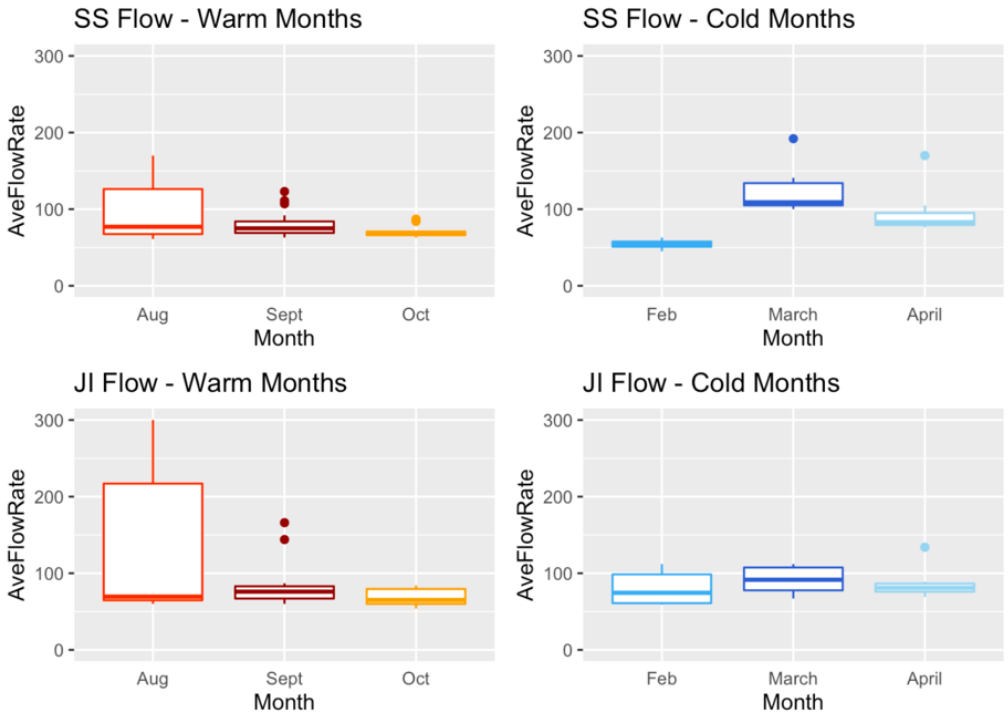

Supplemental Figure 1: The Daily Average Flow measurements (MGD) matching the date of sample collection in SS (top) and JI (bottom) during warmest (left) and coolest (right) months.

Appendix 2. Estimated Decay Rates Based of Negligible Travel Time Decay

The first-order decay rate constant (k) was estimated in R-studio (version 1.4.1103) from linear regression using equations S1. Where C_j and C_s are the concentrations of GC/clinical case-rate in the wastewater at 7.5 hours (JI), and 22 hours (SS), respectively, and k is the decay rate constant.

$$\ln\left(\frac{C_s}{C_j}\right) = -k \times t \quad \text{(S1)}$$

Supplemental Table 2: Estimated decay rates (k/day) of SARS-CoV-2 gram copies (GC) per clinical case per day in wastewater in various flow conditions.

Flow Condition	k (GC/day)
Average	-0.001
Maximum	-0.0004
Minimum	-0.006

Statistics for liner regression of dataset include; residual standard error: 0.663 on 93 degrees of freedom, multiple R-squared: 0.3271, adjusted R-squared: 0.3199, F-statistic: 45.21 on 1 and 93 degrees of freedom, p-value: 1.411e-09.

Appendix 3. Equation of Best-fit for Case Adjusted SARS-CoV-2 Versus Temperature

Case adjusted SARS-CoV-2 concentration (million copies per case) (C_{cp}) throughout different temperatures ranges measured in JI and SS was estimated in R-studio (version 1.4.1103) using equation S2 based on the line of best-fit. Warm and cold months were not broken down into separate data sets due to small numbers of observations.

$$C_{cp} = e^{\beta_0 + \beta_1 T} \quad \text{(S2)}$$

Where T is the average temperature in each specific instance, and β_0 represents the intercept of the regression line when T = 0, and β_1 represents the slope of the regression line.

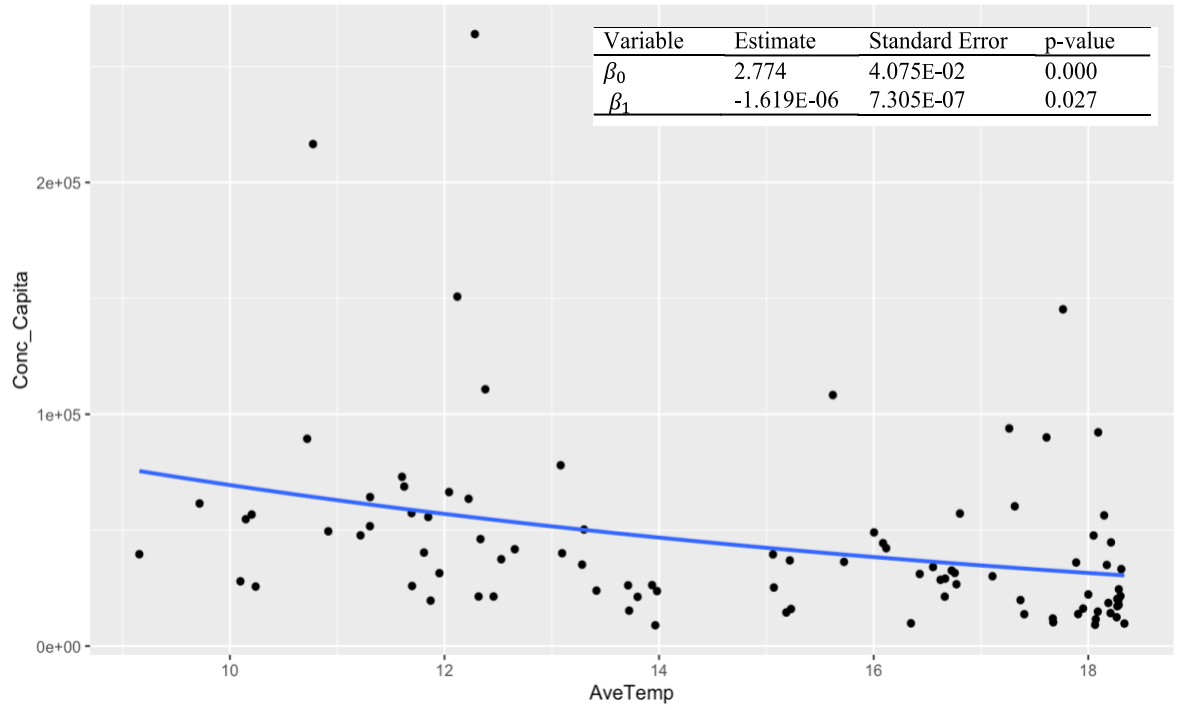

Supplemental Figure 2: Total average case adjusted SARS-CoV-2 concentration (million copies per case) in SS. Line of best fit representing SARS-CoV-2 decay with increasing temperature illustrated in blue. Relevant statistics in top right corner.

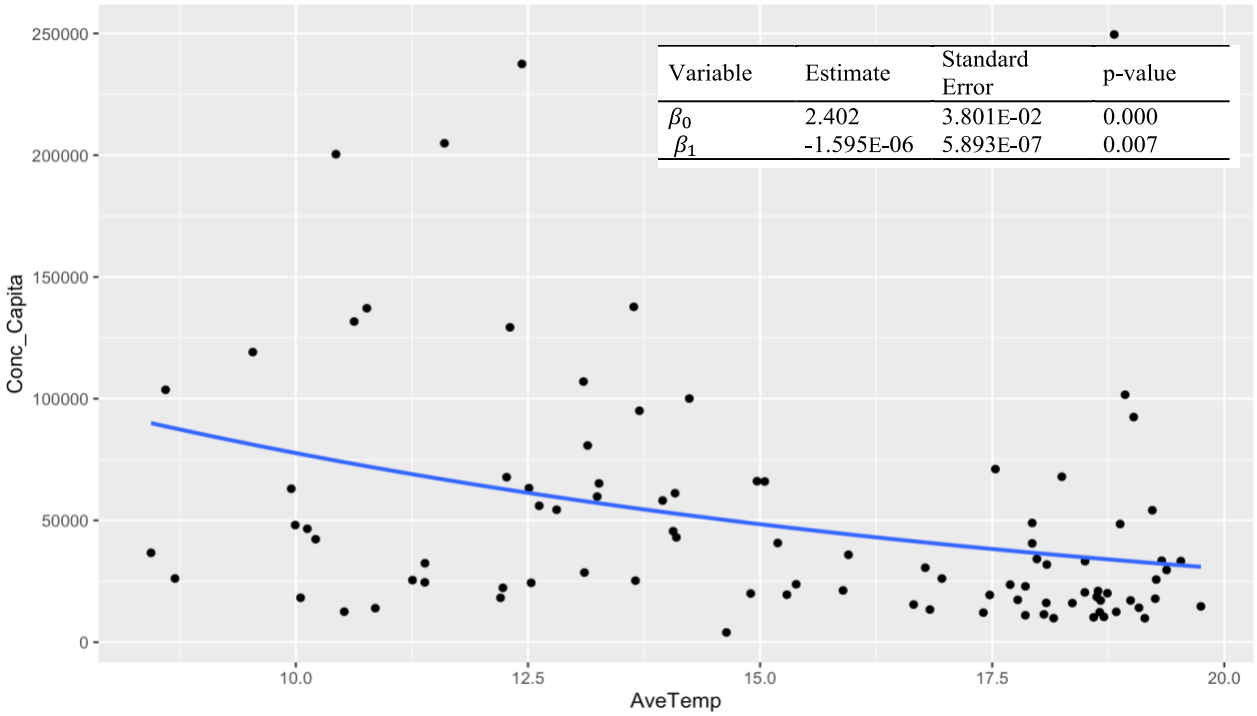

Variable	Estimate	Standard Error	p-value
β_0	2.402	3.801E-02	0.000
β_1	-1.595E-06	5.893E-07	0.007

Supplemental Figure 3: Total average case adjusted SARS-CoV-2 concentration (million copies per case) in JI. Line of best fit representing SARS-CoV-2 decay with increasing temperature illustrated in blue. Relevant statistics in top right corner.